water

MDPI

Article

Dynamics of Sediment Transport and Erosion-Deposition Patterns in the Locality of a Detached Low-Crested Breakwater on a Cohesive Coast

Arniza Fitri [1,*], Roslan Hashim [2,*], Soroush Abolfathi [3] and Khairul Nizam Abdul Maulud [4,5]

1 School of Civil and Architectural Engineering, Nanchang Institute of Technology, Nanchang 330099, China
2 Department of Civil Engineering, Faculty of Engineering, Malaya University, Kuala Lumpur 50603, Malaysia
3 School of Engineering, University of Warwick, Coventry CV4 7AL, UK
4 Earth Observation Centre, Institute for Climate Change, Universiti Kebangsaan Malaysia, Bangi 43600, Selangor, Malaysia
5 Smart and Sustainable Township Research Centre, Faculty of Engineering and Built Environment, Universiti Kebangsaan Malaysia, Bangi 43600, Selangor, Malaysia
* Correspondence: arnizafitri@gmail.com (A.F.); roslan@um.edu.my (R.H.)

Received: 8 June 2019; Accepted: 13 August 2019; Published: 19 August 2019

Abstract: Understanding the dynamics of sediment transport and erosion-deposition patterns in the locality of a coastal structure is vital to evaluating the performance of coastal structures and predicting the changes in coastal dynamics caused by a specific structure. The nearshore hydro-morphodynamic responses to coastal structures vary widely, as these responses are complex functions with numerous parameters, including structural design, sediment and wave dynamics, angle of approach, slope of the coast and the materials making up the beach and structures. This study investigated the sediment transport and erosion-deposition patterns in the locality of a detached low-crested breakwater protecting the cohesive shore of Carey Island, Malaysia. The data used for this study were collected from field measurements and secondary sources from 2014 to 2015. Sea-bed elevations were monitored every two months starting from December 2014 to October 2015, in order to quantify the sea-bed changes and investigate the erosion-deposition patterns of the cohesive sediment due to the existence of the breakwater. In addition, numerical modelling was also performed to understand the impacts of the breakwater on the nearshore hydrodynamics and investigate the dynamics of fine sediment transport around the breakwater structure. A coupled two-dimensional hydrodynamics-sediment transport model based on Reynolds averaged Navier-Stokes (RANS) equations and cell-centered finite volume method with flexible meshing approach was adopted for this study. Analysis of the results showed that the detached breakwater reduced both current speed and wave height behind the structure by an average of 0.12 m/s and 0.1 m, respectively. Also, the breakwater made it possible for trapped suspended sediment to settle in a sheltered area by approximately 8 cm in height near to the first main segment of the breakwater, from 1 year after its construction. The numerical results were in line with the field measurements, where sediment accumulations were concentrated in the landward area behind the breakwater. In particular, sediment accumulations were concentrated along the main segments of the breakwater structure during the Northeast (NE) season, while concentration near the first main segment of the breakwater were recorded during the Southwest (SW) season. The assessment illustrated that the depositional patterns were influenced strongly by the variations in seasonal hydrodynamic conditions, sediment type, sediment supply and the structural design. Detached breakwaters are rarely considered for cohesive shores; hence, this study provides new, significant benefits for engineers, scientists and coastal management authorities with regard to seasonal dynamic changes affected by a detached breakwater and its performance on a cohesive coast.

Keywords: coastal dynamics; coastal resilience; cohesive sediment; detached low-crested breakwater; erosion-deposition pattern; artifitial reef

1. Introduction

Detached breakwaters are parallel barrier structures placed in the shallow nearshore water column, to protect any landform area behind them from the direct impacts of wave attack, currents, tides and storms surges [1,2]. Detached shore-parallel breakwaters are also known as artificial reefs. Low-crest breakwaters have small relative freeboard and are commonly built of quarry materials of homogeneous size [3]. Detached breakwaters are being used increasingly worldwide in the intertidal zones of non-cohesive (sand) coasts, to provide protection measures and mitigate erosion problems [4–7]. However, such coastal structures cause local changes to nearshore flow hydrodynamics and sediment dynamics in the coastal zone [7–9]; these are site-specific and affected by parameters such as sediment characteristics, climate conditions, structural configurations (design, shape, dimension, and material) and nearshore hydro-morphodynamics [2,5,10]. The complexity of morphodynamic changes due to the presence of coastal structures is higher when coastal structures are located on intertidal areas of cohesive shores, where significant temporal and spatial variation of the water depths exist [11].

Sediment transport in coastal areas is mainly influenced by dynamic nearshore processes and site-specific environmental conditions, including sediment characteristics, wind, currents, waves, tides and the exchange processes between estuaries and nearshore regions [12–16]. Coastal protection structures, such as a breakwater, can change flow patterns, hydrodynamics and sediment transport, which could then impact erosion-deposition patterns in the coastal zone [17–19]. Breakwaters can reduce the incident wave energy and impact on the sediment transport capacity, allowing sediment deposition on the shoreward sides of the structure [20,21]. An accurate description of the sediment transport around a protection structure is vital for predicting the effects of coastal structures on morphological changes in coastal zone [22].

Previous studies performed on shoreline changes due to the presence of detached breakwaters have mainly focused on non-cohesive (sand) coasts [23–28], while detached breakwaters are infrequently used at cohesive coasts due to the lack of understanding of complicated cohesive sediment dynamics impacts on nearshore morphodynamics [21,27–29].

The sloping bottom of the nearshore acts like a natural defence and protects the shore against waves, currents and storms [30,31] by dissipating the wave energy through wave breaking phenomena and depending on bottom friction coefficient [32]. The breaking wave may re-form and break again several times before finally rushing up the foreshore areas in the swash zone. However, in the presence of a breakwater in the nearshore area, the structure will interact with incident waves and dissipate some of the wave energy while the remaining turbulent enegy will be reflected and transmitted through the breakwater [33,34]. For submerged breakwater, the waves may simply transmit over the breakwater's structure. However, when the crest of the breakwater is above the mean water level, waves generate a secondary flow at the toe of the structure or transmit through breakwater when the structure is permeable [35].

Previous research has reported that cohesive sediments have low settling velocities and therefore could be transported over a long distance before settling through water column [36–38]. However, the cohesive behaviour of fine sediments allow them to agglomerate and form bigger- sized aggregates called flocks, with higher settling velocities compared to single-particle fine sediments. Thus, flocks can settle in areas where fine sediments can never be deposited [39]. Generally, the formation of flocks can occur when suspended sediments in the water column exceeds 0.01 kg/m^3 [39].

On a non-cohesive shore, presence of breakwaters lead to sand deposition on the lee side of the structure and formation of a sandbar (tombolo) [35,40]. The tombolo grows from the shore towards the structure. Prior to the sand deposition reaching the structure, the sandform is referred to as

salient [35,40]. If a breakwater is built perpendicular to the shoreline, the longshore sediment transport is cut at the breakwater; thus, significant morphological changes occur near the breakwater [22]. For a cohesive shore, the hydro-morphodynamic behaviour of sediments in presence of a detached breakwater is not yet fully understood and more research is needed. This paper provides valuable new information on the dynamic of cohesive sediment in presence of a detached low-crested breakwater, and improves our understanding of the complex hydro-morphodynamics of cohesive coasts which enables coastal planners, managers and engineers, to conduct accurate environmental assessment and design suitable coastal defence structures for cohesive shores.

In the last few decades, the cohesive shore of Carey Island, Malaysia has been experiencing mangrove degradation and erosion problems due to human interventions in the coastal zone. To reduce erosion problems, a rehabilitation project has been carried out by constructing a detached low-crest breakwater near the degraded mangrove area. The impact of the detached breakwater on sediment transport dynamics and erosion-deposition patterns on the cohesive shore had not been fully investigated to this date. Hence, this study aims to understand the sediment transport and erosion-deposition patterns in the locality of a detached low-crested breakwater on the cohesive shore of Carey Island, Malaysia under seasonal variation of hydrodynamic conditions. This study specifically investigates: (i) the characteristics of, and changes in, the hydrodynamics of the cohesive shore of Carey Island due to the existence of the detached breakwater during the NE and SW seasons, (ii) the pattern of suspended sediment concentration (SSC) around the breakwater structure during the NE and SW seasons, and (iii) the variation of sea-bed elevation and the erosion-deposition pattern in the vicinity of the breakwater structure on the cohesive shore of Carey Island.

2. Study Area

The study site is located in degraded environment in an intertidal area of Carey Island on the west coast of peninsular Malaysia, within the Strait of Malacca (Figure 1). The Carey Island coast is a mangrove forest reserve, with a semi-diurnal tidal system that receives daily tidal inundations of maximum 2.96 m MSL of neap rise and 4.33 m MSL of spring rise. For the most part, the Carey Island coast is covered by cohesive sediment. Protection of the landward against tidal inundation and prevention of salt water intrusion during high tides are accomplished by Earth dyke constructed by the Department of Irrigation and Drainage (DID) of Malaysia, along the coastline of the island.

According to the Malaysian Department of Meteorology data, the temperatures at the Carey Island have fluctuated between T_{max} = 35 °C and T_{min} = 26 °C, with an average humidity of 92%, since the year 2000 [40]. Based on the rainfall data collected by the Sime Darby Plantation Berhad in 2015, the total annual rainfall at the study site was 1718 mm and the minimum and maximum monthly rainfalls were 63 mm and 281 mm, respectively (2015). The Langat River is situated near the study site (degraded mangrove area), and the estuary of the river is located approximately 8 km from the study site (Figure 1a). The suspended sediments are carried by Langat River to the Malacca Strait as well as the area of the study site.

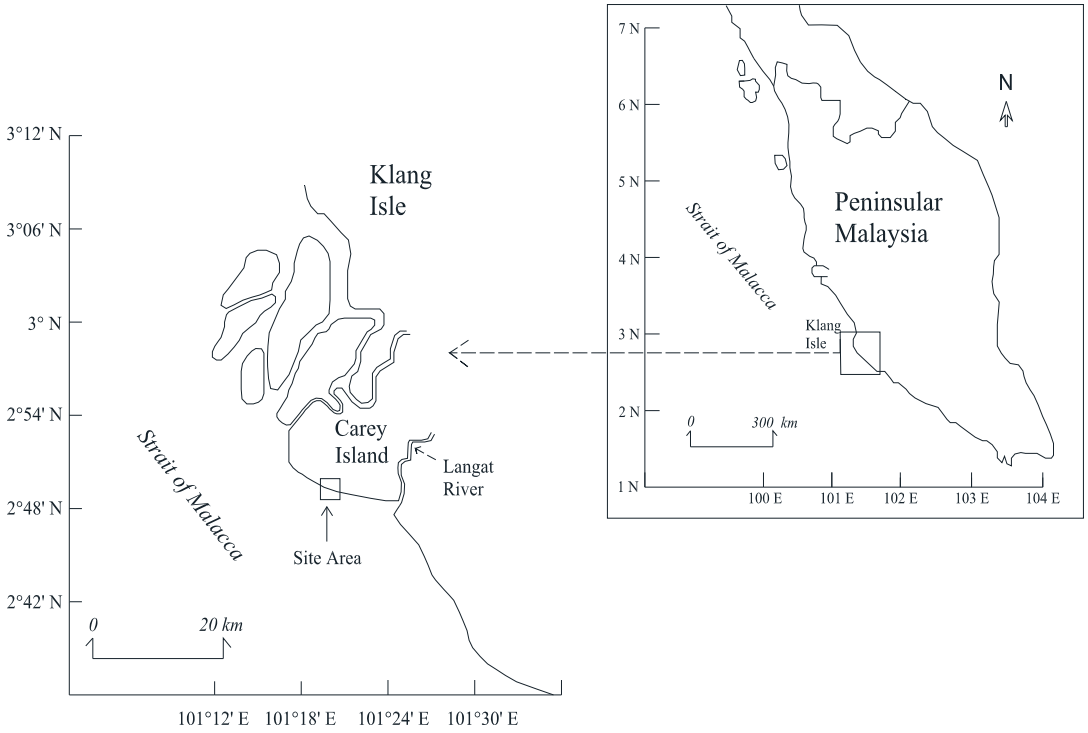

(**a**)

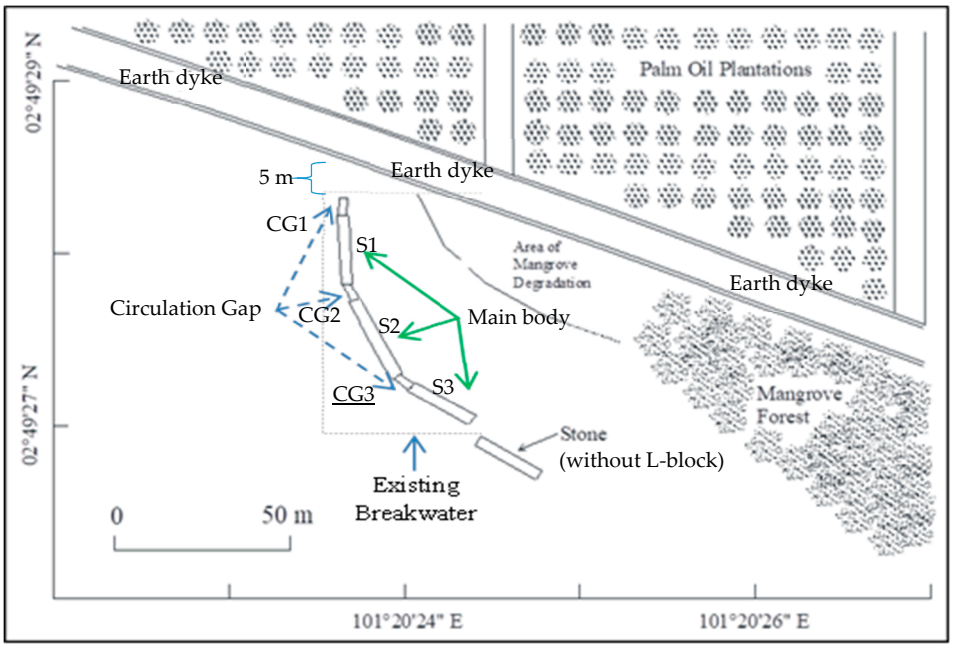

(**b**)

Figure 1. View of the study area: (**a**) location of Carey Island, Malaysia; (**b**) study site.

The problems of erosion and mangrove degradation have plagued the intertidal area of Carey Island since 1995. To tackle this problem, a mangrove rehabilitation project was carried in the intertidal area in early 2009 which included constructing an 85 m-long stretch of low-crested, detached breakwaters consisting of three main segments (main body; S1, S2, S3) and three circulation gaps

(CG1, CG2, CG3) (Figure 1b) [22]. The distance between the dyke structure and the northern section of the breakwater is approximiately 5 m. The lengths of the three main segments of breakwater structure (S1, S2, S3) are 20, 30 and 20 m, respectively, with a height of 1.4 m and a width of 2.5 m. The circulation gaps (CG1, CG2, CG3) are each 5 m long, with a height of 0.8 m, and a width of 2.0 m (Figure 2) [22]. The breakwater was constructed at longitude 101°20′23.5″ to 101°20′24.5″ E, and latitude 02°49′27″ to 02°49′28.5″ N, with the aim reducing current speeds and wave actions and increasing sediment accumulation and sea-bed elevation in the protected mangrove degradation areas behind the breakwater in order to create a suitable tidal regime for restoring the lost mangroves. The detached breakwater is a rubble mound armoured by L-blocks (Figure 2). In addition, there are stones (without L-blocks) with an average diameter of 15 to 20 cm fitted neatly to the right side of the breakwater in mounds approximately 0.8 m high, 2.5 m wide and 20 m long. The stones are arranged to trap more sediment within the study site [22]. The breakwater is submerged during the spring tide and emerges during the neap tide.

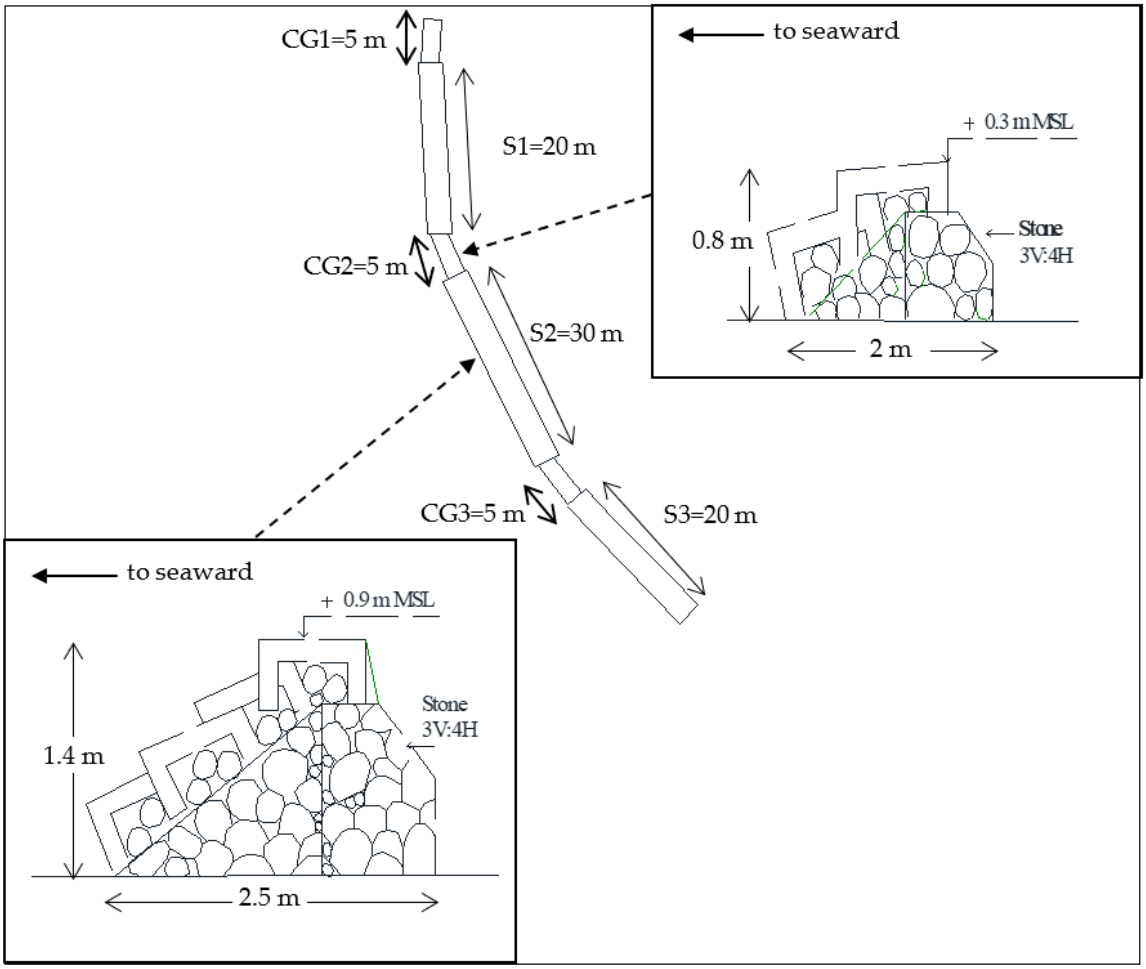

Figure 2. Schematic of detached breakwater structure.

3. Methods

3.1. Data Collection

In this study, field-measured and secondary data were collected and analysed to understand the hydrodynamic and sediment transport patterns. Field-measured data include sediment samplings along the coastline of the Carey Island; fine resolution bathymetry data survey along Langat River and Carey Island coastline; measurement of currents, waves, water level, suspended sediment concentration (SSC) characteristics near the study site area; water samplings at the mouth of Langat River and

near the study site; and monitoring of coastal sea-bed profiles in the vicinity of the breakwaters. The secondary data included the weather data consist of wind and wave data (2014–2015); rainfall data (2014–2015); tide at Lumut station, Belawan station, Tanjung Keling station and Dumai station (2014–2015); and bathymetry data for offshore zones (approximately 45 × 160 km).

The typical weather on Carey Island, Malaysia is primarily influenced by the Northeast season (NE) from November to March and the Southwest season (SW) from May to September. April and October represent transition periods between the two seasons. The weather data, consisting of the daily wind and wave characteristics were collected at lat. 2°–3° N, long. 101°–102° E by the Malaysian Department of Meteorology. The 3-hour wave climate conditions were also obtained from the European Centre for Weather Forecasts of Medium Range (ECMWF), in grid format for longitude 99.75° E–101.45° E and latitude 2° N–3.25° N. Hourly rainfall data for the Klang region was obtained from the West Estate Office, Sime Darby Plantation Berhad, Carey Island, and hourly tidal data was obtained from the Malaysian Survey and Mapping Department (JUPEM). Figure 3 presents the wind roses during the NE and SW seasons based on the analysis of weather data in 2015. The figure illustrates the dominant wind speed and direction during both NE and SW seasons. The weather data were used for setting up the hydrodynamic conditions in the numerical modelling study (Section 3.3).

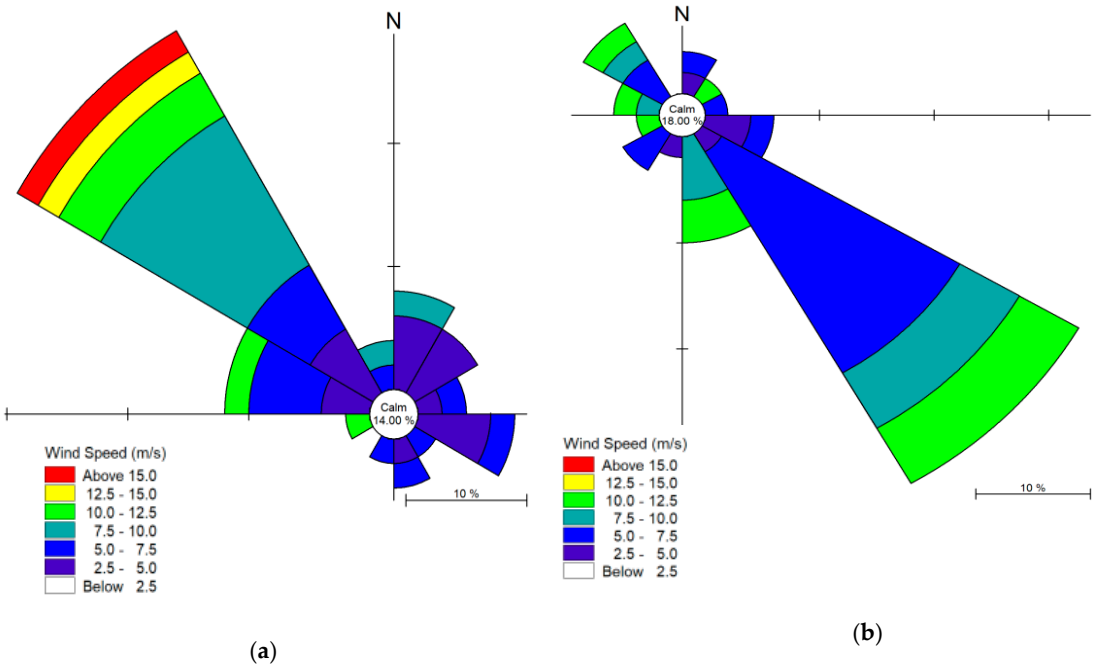

Figure 3. Wind roses in 2015: (**a**) NE season; (**b**) SW season (sources of data: Malaysian Department of Meteorology).

During the field measurement campaign, twenty sediment samples were collected along the Carey Island coastline and the area surrounding the breakwater, at depths of 0–100 cm to determine the size distribution of the sediment particles.

Water samples and flow velocity were collected from the mouth of the Langat River (during the period of 23 December 2014 to 7 January 2015) to determine the total suspended solids (TSS1) values and the discharge values of the river. For each TSS test, 100 mL water of each sample was filtered through a pre-weighed glass fibre filter. The filters were then dried at 105 °C in an oven and weighed. The mass differences between the pre and post-filtration of the filter were measured to determine the total suspended sediment in 100 mL of water. The TSS analyses were performed in accordance with the APHA 2540D standard method. Furthermore, in order to obtain information about the average amount of TSS in the Strait of Malacca (TSS 2), which can affect the sediment transport around the study site, ten water samples were collected monthly from a site located at latitude 2°49′38.38″ N and longitude

101°19′55.39″ E, which is approximately 500 m seaward of the breakwater. Table 1 summarises the monthly climate conditions at the study site in 2015.

Table 1. Monthly climate conditions in 2015.

	Month											
	Jan	**Feb**	**Mar**	**Apr**	**May**	**Jun**	**Jul**	**Aug**	**Sep**	**Oct**	**Nov**	**Dec**
No. of rainfall events	4	5	4	5	9	4	4	12	7	9	11	14
Rainfall (mm/month)	63	64	118	60	221	128	65	281	254	139	192	133
Significant wave height (m)	1.2	0.75	1	1	0.75	0.75	0.5	0.75	1	1.5	1.2	1
Mean wave period (s)	5	4	5	4	3	3	3	4	5	5	5	4
Dominant wind speed (m/s)	9.1	7.5	8.5	7.3	6.2	5.3	5.5	6.5	5.0	6.5	7.5	8.5
Dominant wind direction (degree)	300	330	320	270	120	130	140	130	120	290	310	300

Sources of data: Rainfall data were obtained from Sime Darby Plantation Berhad, Carey Island; Wind and wave data were obtained from Malaysian Meteorology Department and ECMWF.

Based on weather data obtained from Malaysian Meteorology Department (Figure 3), the wind during the NE season predominantly blew from the Northwest (approximately 300°–330°) at a dominant speed range of 7.5–10 m/s, while the wind during the SW season predominantly blew from a Southeastern direction (approximately 120°–150°) at a dominant speed range of 5–7.5 m/s. Monthly climate monitoring (Table 1), indicates the significant wave heights and intensity of wind speed were higher during the Northeast season compared to the Southwest season.

In addition to the climatic data mentioned above, two Acoustic Wave and Current Profiler (AWAC) units and four optical backscatter sensors (OBS-3A) were installed at the study site (see Figure 4) to measure the suspended sediment concentration (SSC), water level fluctuations, currents and waves characteristics. Field measurements using AWAC and OBS-3A were carried out from 23 December 2014 to 7 January 2015, covering both the neap and spring tides. The data collected during the field study campaign, were used for the model setup, calibration and validation of the numerical model (Section 3.3). Table 2 shows the coordinates and water depth for the AWACs, OBS-3As, water samples and water discharge measurements.

Table 2. Coordinates of field measurements.

Station	**Longitude (x)**	**Latitude (y)**	**Water Depth (m)**
Station 1 (AWAC 1 and OBS 1)	101°20′11.18″ E	02°48′40.02″ N	10.324
Station 2 (AWAC 2 and OBS 2)	101°18′58.14″ E	02°49′26″ N	12.557
Station 3 (OBS 3)	101°26′10.06″ E	02°40′7.91′ N	15.221
Station 4 (OBS 4)	101°06′44.34″ E	03°8′36.81″ N	10.483
Water samples (TSS 1) and water discharges from LR	101°24′6.24″ E	2°48′2.72″ N	6.242

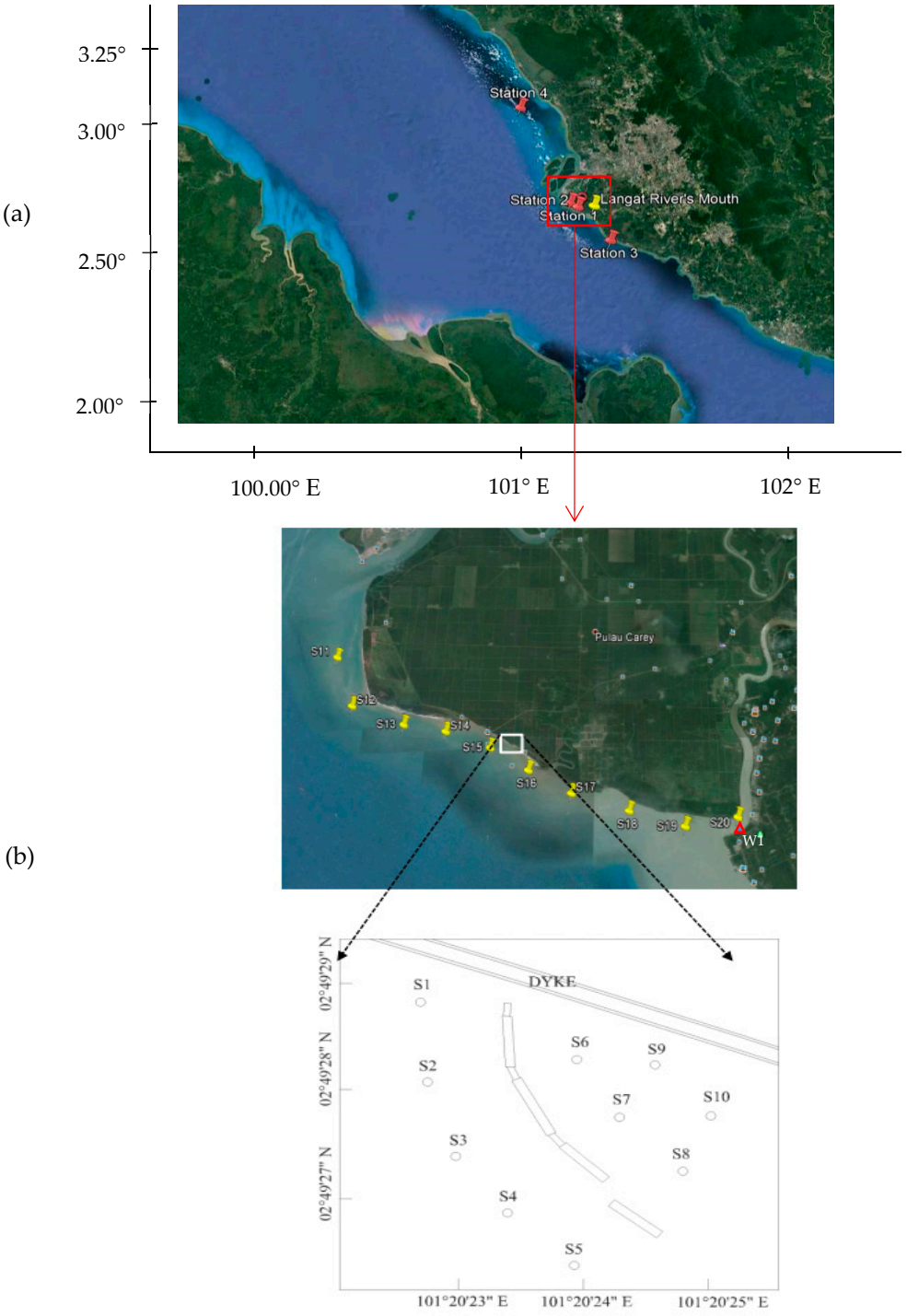

Figure 4. (**a**) Locations of AWAC and OBS-3A units within the study site, (**b**) location of water and bed samples in the study site (S = soil sample, W = water sample and discharge).

A fine resolution bathymetry survey was conducted around the coastline of Carey Island and the Langat River, covering an area of 17.5 × 5 km with lines spaced at 20–500 m intervals. The survey was carried out using a boat equipped with an echo-sounder and a DGPS during the spring tide on 8 to 12 December 2014. Bathymetry data were processed and prepared for setting up the numerical model using flexible meshing technique.

3.2. Monitoring of Sea-Bed Elevation

The sea-bed elevations in the mangrove degraded area of the Carey Island intertidal region were monitored using a Total Station (theodolite) and bed-profiler for a two-month period, during the period from December 2014 to October 2015. The sea-bed elevation monitoring was mainly concentrated at the breakwater region, especially the mangrove degraded area at the landward of the breakwater, as more significant sea-bed level changes was expected in that area. A total of twenty-four profile lines (CS1 to CS24), perpendicular to the shoreline, were surveyed and monitored during the study period (Figure 5). Monitoring sea-bed levels on a cohesive shore is a difficult task since any movement on the cohesive sea-bed could disturb the sediment surfaces significantly. In this study, wooden poles were pushed into the cohesive sediments around the monitoring area at 5 m distances along each profile line to obtain accurate bed surface data. The bed profile measurements were conducted during low tide exposure, according to the datum provided by JUPEM near the study site. The profiling outcomes were used to analyse the erosion-deposition patterns in the locality of the breakwater's structure by determining the elevation differences between the bed profiling measurements obtained and the initial sea-bed elevations in December 2014.

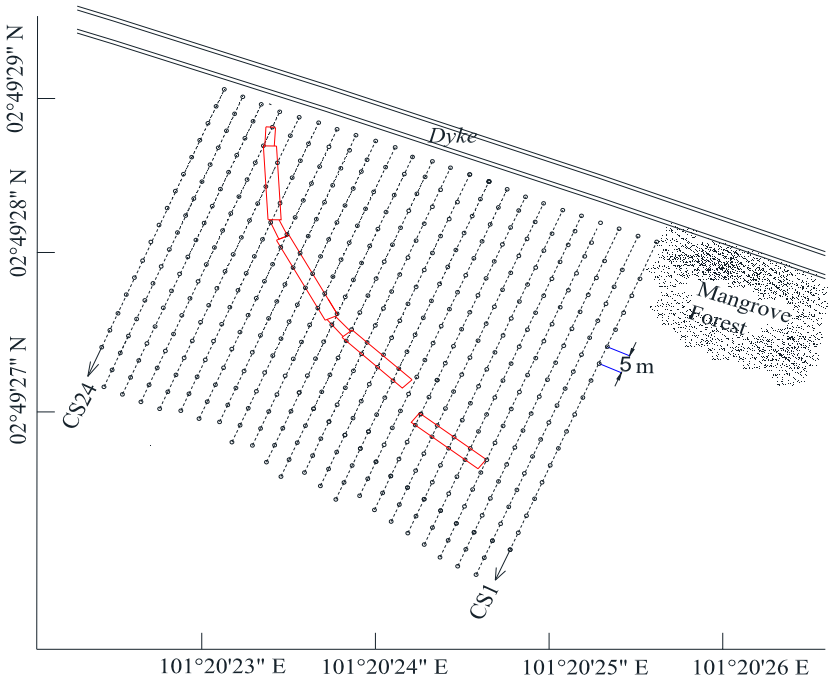

Figure 5. Bed profiling method in the study site (24 profiles).

3.3. Numerical Modelling

Accurate prediction of hydrodynamic and sediment transport characteristics under the influence of wave-current interactions in coastal regions is a challenging task due to multifaceted nearshore dynamic processes which are varying on both temporal and spatial scales [19,41,42]. Previous studies have shown that modelling nearshore problems based on the shallow water equation provides high accuracy and efficiency [11,43,44]. In this study, the MIKE 21 Flow Model FM including Hydrodynamic, Spectra Wave and Mud Transport modules was adopted for simulating the flow hydrodynamics and cohesive sediment transport for the case study described in Section 2. MIKE 21 Flow model FM is a complete coastal modelling suite, which is capable of designing the data assessment for coastal and offshore structures; and environmental impact assessment of marine infrastructures based on flexible mesh approach. This model was established by the Danish Hydraulic Institute (DHI), Denmark. MIKE 21 Hydrodynamic is the basic module of the MIKE 21 Flow Model FM system for free surface flows which simulates water level fluctuations and flows in response to a variety of forcing functions

in lakes, estuaries, bays and coastal areas. The details of the numerical model used for this study are as follows:

The modelling approach adopted for this study is based on the numerical solution of the two dimensional incompressible Reynolds averaged Navier-Stokes equations with the assumption of Boussinesq and hydrostatic pressure.

The governing equations used for the two-dimesional numerical model in Cartesian coordinates are continuity (Equation (1)) and momentum (Equations (2) and (3)):

$$\frac{\partial u}{\partial x} + \frac{\partial v}{\partial y} + \frac{\partial w}{\partial z} = S \tag{1}$$

$$\frac{\partial u}{\partial t} + \frac{\partial u^2}{\partial x} + \frac{\partial vu}{\partial y} + \frac{\partial wu}{\partial z} = fv - g\frac{\partial \eta}{\partial x} - \frac{1}{\rho_0}\frac{\partial p_a}{\partial x} - \frac{g}{\rho_0}\int_z^\eta \frac{\partial \rho}{\partial x}dz + F_u + \frac{\partial}{\partial z}\left(\nu_t \frac{\partial u}{\partial z}\right) + u_s S \tag{2}$$

$$\frac{\partial v}{\partial t} + \frac{\partial v^2}{\partial y} + \frac{\partial vu}{\partial x} + \frac{\partial wu}{\partial z} = -fu - g\frac{\partial \eta}{\partial y} - \frac{1}{\rho_0}\frac{\partial p_a}{\partial y} - \frac{g}{\rho_0}\int_z^\eta \frac{\partial \rho}{\partial y}dz + F_v + \frac{\partial}{\partial z}\left(\nu_t \frac{\partial v}{\partial z}\right) + u_s S \tag{3}$$

where t denotes time and u, v, w are velocity components in x, y, z Cartesian coordinates, respectively. d denotes the still water depth and h is the total water depth ($= \eta + d$), g is the gravitational acceleration, p_a is atmospheric pressure, ρ is density, ρ_0 is reference density of water, ν_t is the vertical diffusivity, f is Coriolis parameter and S is point-source discharge magnitude. F_u and F_v are gradient-stress relations described is Equations (4) and (5), respectively.

$$F_u = \frac{\partial}{\partial x}(2A\frac{\partial u}{\partial x}) + \frac{\partial}{\partial y}\left(A\left(\frac{\partial u}{\partial y} + \frac{\partial v}{\partial x}\right)\right) \tag{4}$$

$$F_v = \frac{\partial}{\partial x}\left(A\left(\frac{\partial u}{\partial y} + \frac{\partial v}{\partial x}\right)\right) + \frac{\partial}{\partial y}\left(2A\frac{\partial v}{\partial y}\right) \tag{5}$$

where A is the horizontal eddy viscosity.

The total water depth, h is determined based on the kinematic boundary condition at the surface by use of robust vertical integration of local continuity equation (Equation (6)).

$$\frac{\partial h}{\partial t} + \frac{\partial h\overline{u}}{\partial x} + \frac{\partial h\overline{v}}{\partial y} = hS + \hat{P} - \hat{E} \tag{6}$$

where $\hat{P}$ and $\hat{E}$ are the precipitation and evaporation rates, respectively and $\overline{u}$ and $\overline{v}$ are the depth-averaged velocities in the two-dimensional domain. The model does not consider compressibility of water. A standard $k - \varepsilon$ model is used for turbulence modelling and the vertical eddy diffusivity is derived based on Equation (7).

$$\nu_t = c_\mu \frac{k^2}{\varepsilon} \tag{7}$$

where k is the turbulent kinetic energy per unit mass, c_μ is an empirical constant and ε is the dissipation rate of turbulent kinetic energy.

The discretisation of the numerical domain is performed with use of unstructured grid approach to achieve an optimal degree of flexibility in the representation of geometry of the detached breakwater, enabling a smooth representation of offshore and onshore boundaries. The flexible meshing approach used for this study enabled depth-adaptive and boundary-fitted mesh and provided adequate resolution of the bathymetry of study site, as well as high accuracy wave and current generation. MIKE 21 Spectral Wave (SW), a spectral wind-wave model, is used to simulate the growth, decay and transformation of wind-generated waves and swells in the numerical domain for the described case-study. The model solves the spectral wave action balance equation formulated by Komen et al. [45] and Young [46].

The hydrodynamic module was coupled with a sediment transport module capable of simulating fine sediments, to investigate the impact of detached breakwater on the coastal waters of Carey Island

and the sediment deposition-erosion patterns landwards of the breakwater. MIKE 21 Mud Transport module solves an advection-dispersion equation, based on Mehta [47], and the impact of waves and currents are introduced with bed shear stress. The cohesive sediment transport is described by Equation (8):

$$\frac{\partial c^i}{\partial t} + \frac{\partial uc^i}{\partial x} + \frac{\partial vc^i}{\partial y} + \frac{\partial wc^i}{\partial z} - \frac{\partial w_s c^i}{\partial z} = \frac{\partial}{\partial x}\left(\frac{\nu_{Tx}}{\sigma^i_{Tx}}\frac{\partial c^i}{\partial x}\right) + \frac{\partial}{\partial y}\left(\frac{\nu_{Ty}}{\sigma^i_{Ty}}\frac{\partial c^i}{\partial y}\right) + \frac{\partial}{\partial z}\left(\frac{\nu_{Tz}}{\sigma^i_{Tz}}\frac{\partial c^i}{\partial z}\right) + S^i \quad (8)$$

where c^i is the i^{th} component of the mass concentration, ν_{Tx} is the anistropic eddy viscosity, S^i is the source term, σ^i_{Tx} is turbulent Schmitt number, and w_s is the settling velocity. The model is capable of considering flocculation as a function of suspended sediment concentration (Equation (9)).

$$w_s = k \times \left(\frac{c}{\rho_{sediment}}\right)^{\gamma} \quad (9)$$

where k is a constant, $\rho_{sediment}$ is sediment density, and γ is the settling index coefficient. The deposition is described in the model by Equation (10):

$$S_D = w_s c_b p_D \quad (10)$$

where w_s denotes settling velocity of suspended sediment, p_D describes the probability of deposition ($= 1 - \tau_b/\tau_{cd}$) and c_b is suspended sediment concentration near the bed. The sediment transport model is soved by spatial discretisation of the primitive equations with use of cell-centred finite volume method. An unstructured gird approach is used for the horizontal plane, while in the vertical domain structured mesh is used.

The numerical model described above has been adopted successfully in several studies. Jose and Stone [48] and Jose et al. [49] investigated the characteristics of wave transformation with MIKE 21 Spectra Wave model for south-central Louisiana, USA [49]. Patra et al. [44] investigated and validated the characteristics of offshore waves in the Bay of Bengal, India using MIKE 21 Spectra Wave FM. In addition, a study of suspended sediment transport was carried out sucessfully by Sravanthi et al. [10] along the cohesive shore of Central Kerala, India using MIKE 21 Mud Transport FM. Previous studies have shown that MIKE 21 is capable of simulating hydrodynamic processes with over 85% accuracy when compared to field data [11,44,48–50].

3.3.1. Model Setup

The numerical model described in Section 3.3 is used to investigate the impact of breakwater on the hydrodynamics and sediment transport patterns in the locality of the breakwater. In this study, the hydrodynamic characteristics, including currents and waves, were simulated in presence of the breakwater and without the breakwater for both seasons (northeast season and southwest season) to quantify the impact of the breakwater on the nearshore processes. Separate models were developed to simulate the conditions for the neap and spring tides. The suspended sediment concentrations (SSCs) were also simulated in the vicinity of the breakwater for both seasons and tidal conditions. The numerical results were compared to the data obtained from field measurements, for calibration and validation purposes.

3.3.2. Model Input

Model input data consisted of bathymetry data; climate data, including wind characteristics, water level and wave characteristics; sediment data, including sediment characteristics, SSC and TSS; and water discharge from the Langat River. The bathymetry data for the Strait of Malacca at coarse resolution were obtained from the Malaysian National Hydrography Centre, based on navigation survey from 2012. These data were further integrated with bathymetry data provided by DHI in

C-MAP (2014). Bathymetry data for the Carey Island coast and Langat River areas were measured at fine resolution during the fieldwork (8 to 12 December 2014). Following successful model calibration and validation, the NE season simulations were set up by using the dominant wind (8.5 m/s of speed and 310° of direction) and wave characteristics (1 m height and 5 s period) during the NE season in 2015 and the average SSC. For the SW season simulations, the model was set up by using the dominant wind (6.5 m/s of speed and 140° of direction) and wave characteristics (0.75 m height and 3 s period) during SW season in 2015 and the average SSC. Both models used SSC data collected from 23 December 2014 to 7 January 2015.

3.3.3. Computational Domain

The computational domain was developed with the use of bathymetry data and by adopting a flexible mesh technique. Figure 6 depicts the computational domain developed for hydrodynamic and sediment transport modelling. This study set the computational domains beyond the study area, according to the guideline for coastal hydraulic studies published by the Department of Irrigation and Drainage (DID), Malaysia [51]. Therefore, the computational domain developed for the simulation (MIKE 21 Hydrodynamic and MIKE 21 Spectra Wave) was expanded to include the Tanjung Keling and Lumut areas (Figure 6a). To improve the cost efficiency of the modelling, smaller computational domain were generated for the sediment transport model (Figure 6b). Figure 6 depicts the computational domain developed for hydrodynamic, wave and sediment transport modelling.

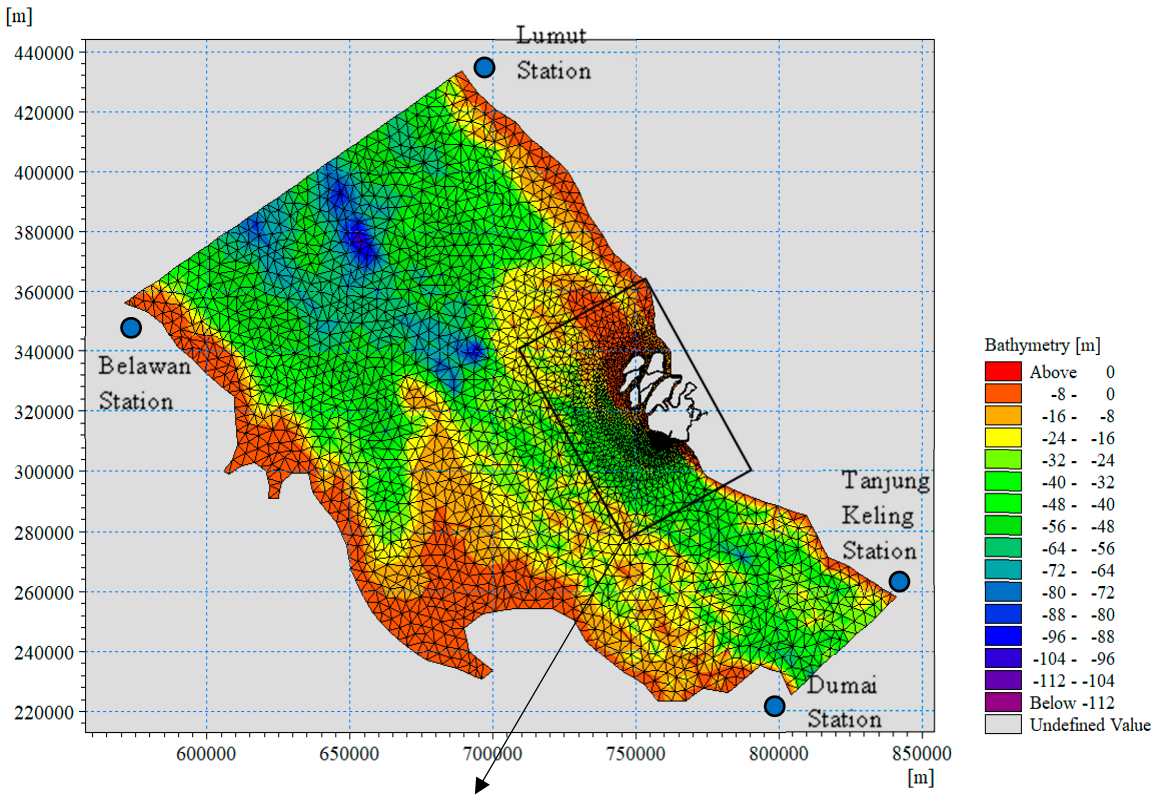

(**a**)

Figure 6. *Cont.*

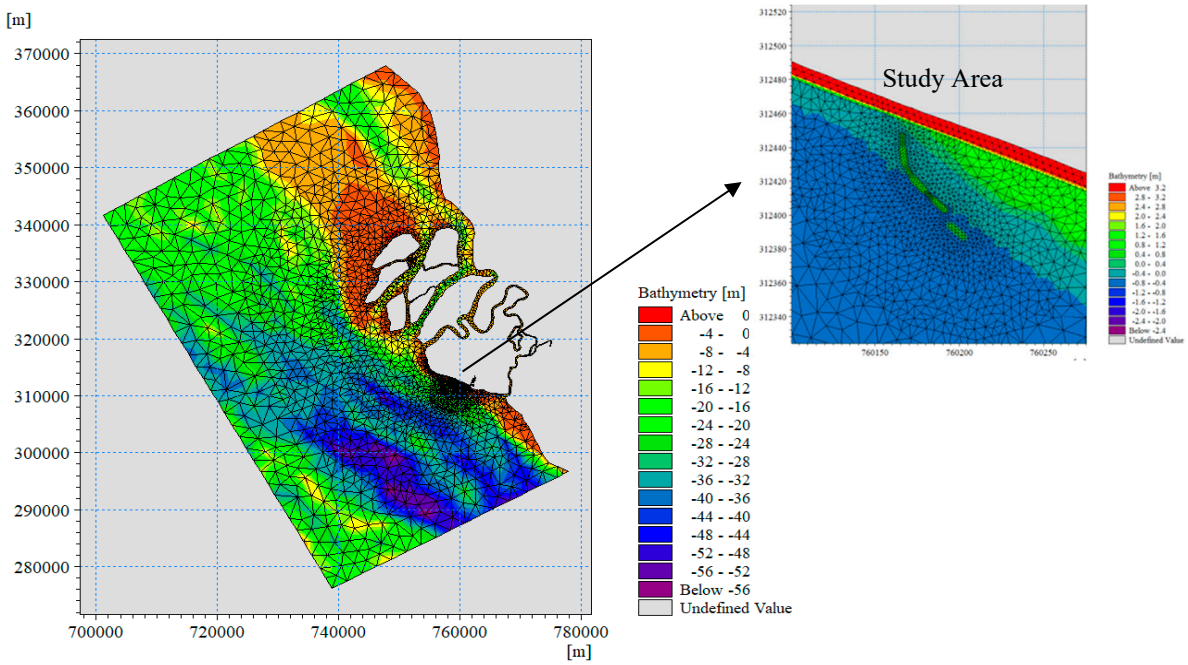

Figure 6. Computational domain: (**a**) hydrodynamic and wave models; (**b**) mud transport model.

3.3.4. Model Calibration and Validation

To check the accuracy of the simulation results from the models and to provide confidence in the simulations of the current, waves and patterns of suspended sediment concentration in the locality of the existing detached breakwater, the simulation results obtained from the models were calibrated initially against measured conditions on 23 December 2014 to 7 January 2015 at station 1 (lat: 02°48′40.02″ N, long: 101°20′11.18″ E). The models were further validated against field measurements taken between 23 December 2014 and 7 January 2015 at station 2 (lat: 02°49′26″ N, long: 101°18′58.14″ E.

The calibration of the hydrodynamic model was carried out by adjusting the values of the bed roughness/Manning number over the whole computational domain [52]. The calibration of the spectra wave model was carried out by adjusting the values of the wave breaking parameters, bottom friction parameters and white-capping (deep water wave breaking) parameters [53]. The calibration of the mud transport model was carried out by adjusting the values of the erosion coefficient, power of erosion, settling velocity and critical shear stress for deposition and erosion [39]. To check the accuracy of the simulation results, the Theil's inequality coefficients, R Squared (R^2), and Root Mean Squared Error (RMSE) were calculated [44,48,54].

Figure 7 compares the simulated and measured water level, current characteristics, wave characteristics and SSC at station 1. Figure 8 depicts the comparison between the simulated and measured water level, current characteristics, wave characteristics and SSC at station 2. Table 3 presents the values of Thiel's coefficient, R^2 and RMSE obtained during the model calibration and validation. Based on the standard error allowed by the DID (2013) for hydrodynamic and sediment transport modelling, the values proved that the models were calibrated and validated well.

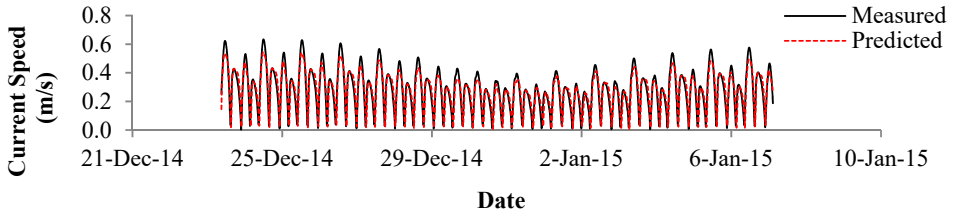

(a)

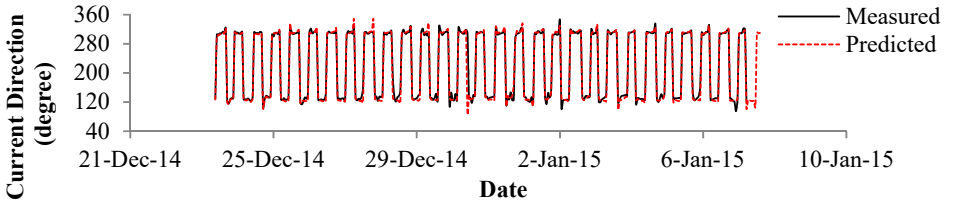

(b)

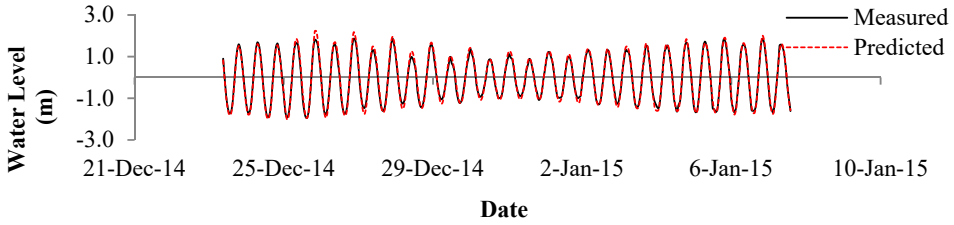

(c)

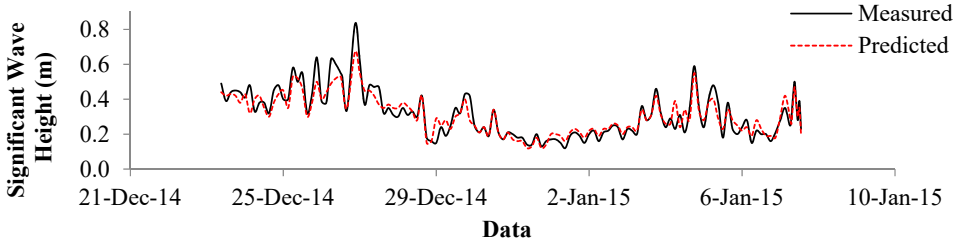

(d)

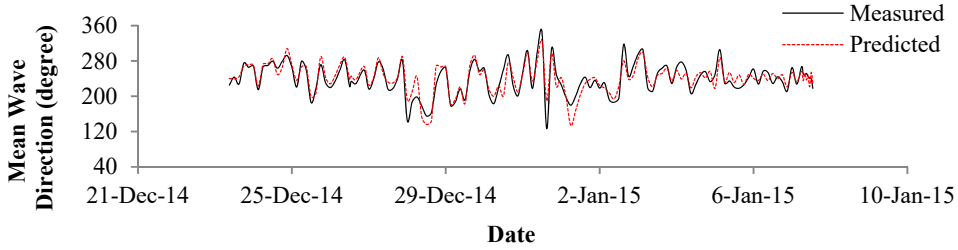

(e)

Figure 7. *Cont.*

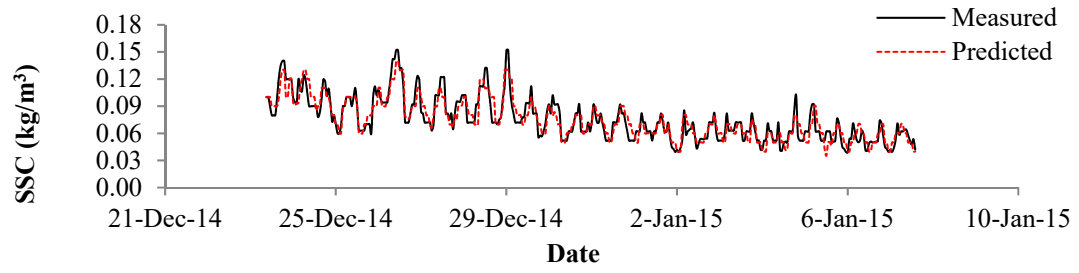

(f)

Figure 7. Comparison between simulation results and field measurements on 23 December 2014 to 7 January 2015 at station 1 (long: 101°20′11.18″ E, lat: 02°48′40.02″ N), (**a**) current speed; (**b**) current direction; (**c**) water level; (**d**) significant wave height; (**e**) mean wave direction; (**f**) SSC.

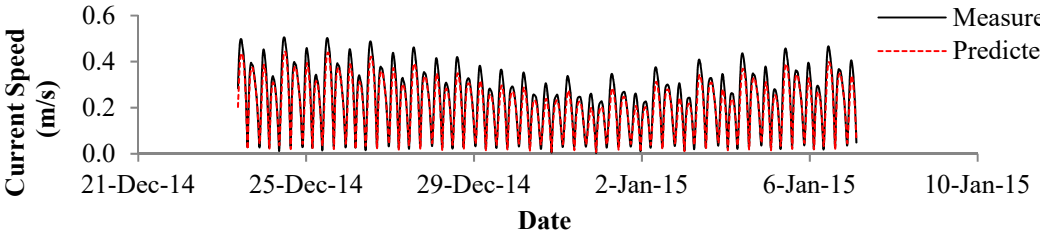

(a)

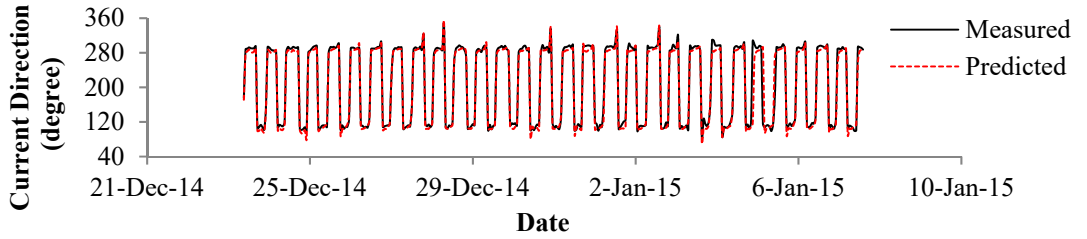

(b)

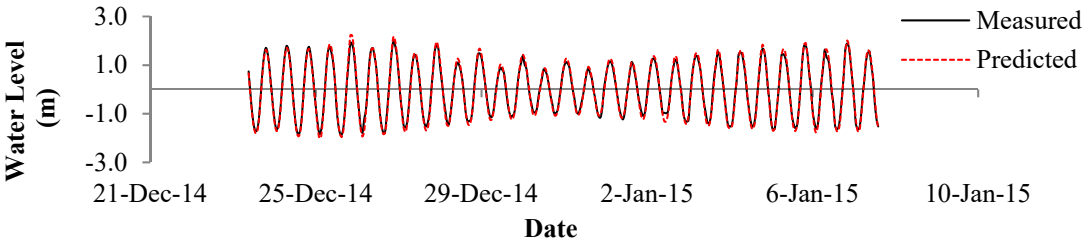

(c)

Figure 8. *Cont.*

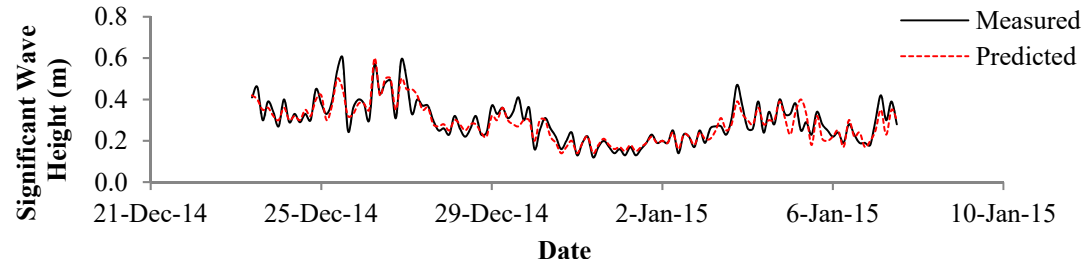

(d)

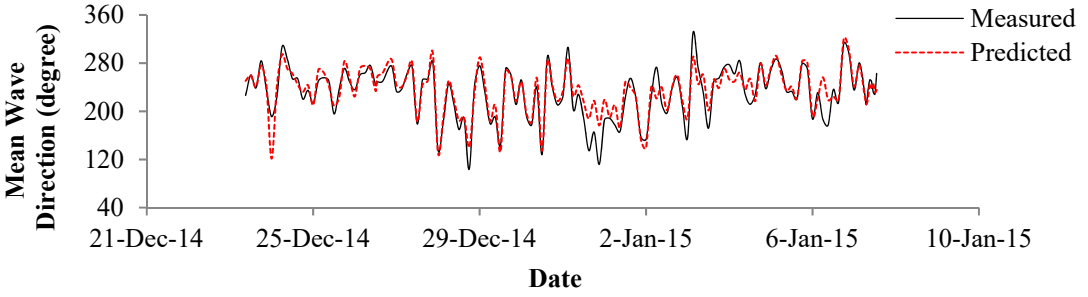

(e)

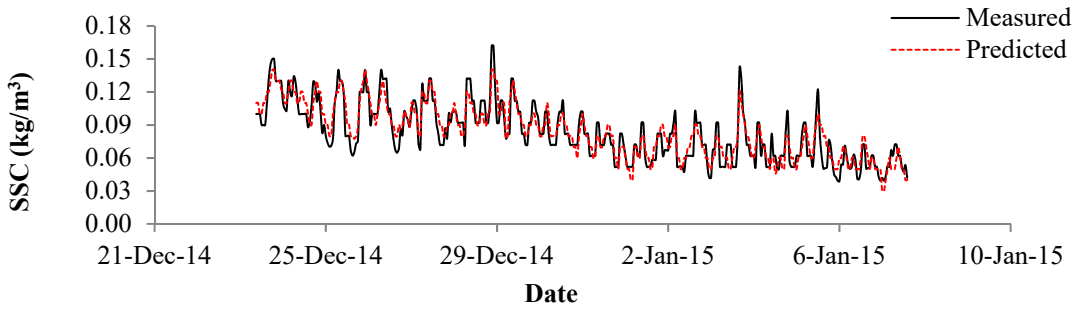

(f)

Figure 8. Comparison between simulation results and field measurements on 23 December 2014 to 7 January 2015 at station 2 (long: 101°18′58.14″ E, lat: 02°49′26″ N), (**a**) current speed; (**b**) current direction; (**c**) water level; (**d**) significant wave height; (**e**) mean wave direction; (**f**) SSC.

Table 3. Statistical results for the performance of the hydrodynamic, wave and mud transport models.

Parameter	Calibration			Validation		
	RMSE	R Squared (R^2)	Thiel's Inequality Coefficient	RMSE	R Squared (R^2)	Thiel's Inequality Coefficient
Current Speeds	0.07 m/s	0.92	0.08	0.08 m/s	0.91	0.08
Current Directions	15°	0.94	0.05	17°	0.93	0.06
Water Levels	0.05 m	0.95	0.04	0.06 m	0.94	0.05
Significant wave heights	0.04 m	0.85	0.14	0.05 m	0.83	0.16
Mean Wave Directions	18°	0.81	0.18	19°	0.80	0.19
SSC	0.004 kg/m^3	0.83	0.16	0.005 kg/m^3	0.82	0.17

4. Results and Discussion

4.1. Sediment and Water Samples Analyses

According to the results of sediment particle analyses, the median grain diameter (D_{50}) of the cohesive sediments in the intertidal area of Carey Island, at depth of 0–40 cm, was determined to be 0.015–0.022 mm, which was consisted of 10% clay, 71% silt and 19% fine sand. Furthermore, the sediment fraction at depths of 40–100 cm consisted of stiff clay. Based on water samples and velocity measurements at the mouth of the Langat River, TSS 1 showed that the Langat River carries 180–261 mg/L of suspended sediments to the Malacca Strait with 698–1130 m^3/s of water discharges during ebb tide and 121–479 m^3/s during spring tide. Table 4 present TSS 2 analyses from the water samples collected at 500 m seaward of the breakwater.

Table 4. Monthly amount of TSS 2 in 2015.

	Month											
	Jan	**Feb**	**Mar**	**Apr**	**May**	**Jun**	**Jul**	**Aug**	**Sep**	**Oct**	**Nov**	**Dec**
TSS 2 (kg/m^3)	0.047	0.043	0.058	0.049	0.079	0.071	0.06	0.081	0.076	0.058	0.061	0.056

Table 4 shows that the amounts of TSS2 were higher during the Southwest season, when the monthly rainfall intensities were also higher (see Table 1). High concentration of suspended sediment from the Langat River into the Strait of Malacca is expected during the Southwest season, due to the higher rainfall intensities. The wind from the Southeast direction transports the suspended sediment from the mouth of the Langat River to the study site.

4.2. Hydrodynamic Changes in the Locality of the Breakwater Structure

Figure 9 illustrates the simulation results for the currents and waves characteristics with and without the breakwater during the NE season, for the maximum tidal level of the neap tide and spring tide conditions. Figure 10 presents the simulation results for the currents and waves characteristics with and without the breakwater during SW season for the maximum tidal level of the neap tide and spring tide conditions.

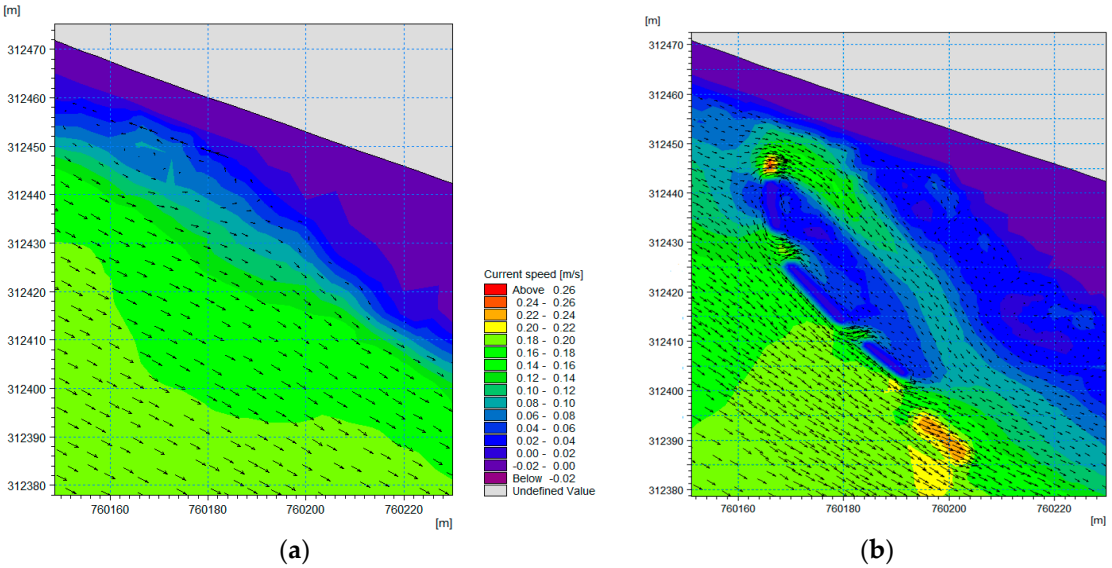

Figure 9. *Cont.*

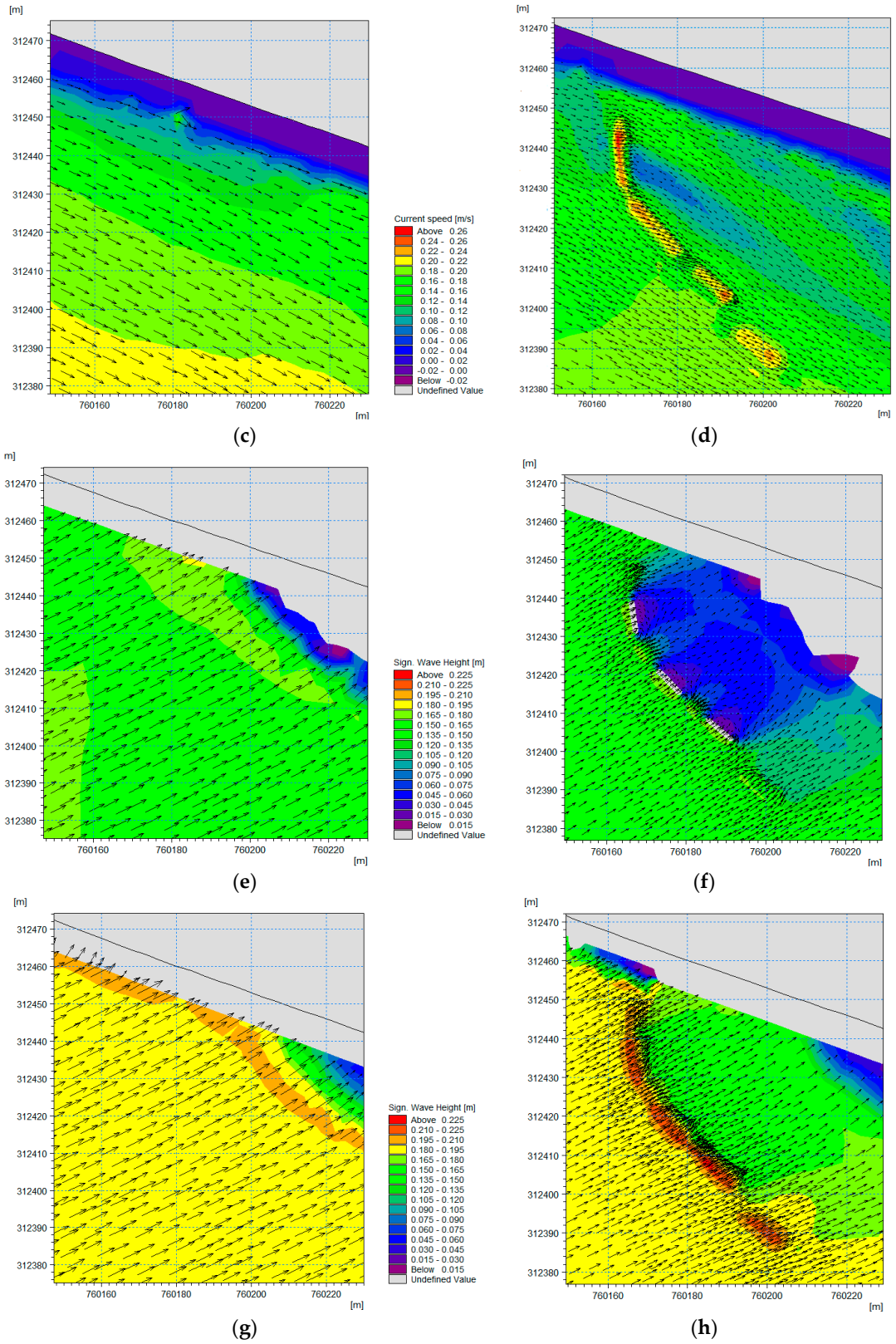

Figure 9. Simulated current and wave characteristics during the Northeast season: (**a**) CS during NT (WT); (**b**) CS during NT (W); (**c**) CS during ST (WT); (**d**) CS during ST (W); (**e**) SWH during NT (WT); (**f**) SWH during NT (W); (**g**) SWH during ST (WT); (**h**) SWH during ST (W). Notes: W = with breakwater, WT = without breakwater, CS = current speed, SWH = significant wave height, NT = neap tide, ST = spring tide.

(a) Changes in Current and Wave Characteristics during the Northeast Season (NE)

The simulation results shown in Figure 9 demonstrate that during the NE season and without the existence of the breakwater structure, the currents flow directly to the study site (degraded mangrove area) from a Northwest direction at approximately 300° to 330° (magnetic) towards the Southeast direction with velocity between 0.12 and 0.22 m/s. At the same time, incident waves impose force on the mangrove degradation areas from a Southwest direction at approximately 230° to 250° (magnetic) to the Northeast direction, with the significant wave heights between 0.10 and 0.21 m. In addition, the simulation results also show that the current velocity and wave heights were reduced in the nearshore area, before reaching the study site, due to the resistance forces of the cohesive sediment. Previous studies have reported that cohesive bed slopes have higher friction coefficients compared to sandy beach slopes [30,31]. Therefore, current and wave turbulent energies are reduced on cohesive coastal bed slopes.

Due to the presence of the breakwater at the study site, the current and wave characteristics changed dynamically around the degraded mangrove area. For the maximum tidal level during neap tide conditions, the water levels were lower than the main segment's (S1, S2, S3) crest levels and higher than circulation gaps' (CG1, CG2, CG3) crest levels (the breakwater was not submerged). Currents and waves entered the mangrove degradation area via overtopping the circulation gap's (CG1, CG2, CG3) of the breakwater and through the available gaps between the breakwater and earth dyke or between the breakwater and the stone (without L-blocks). At this moment, the current speeds on the landward side of the breakwater decreased from 0.18 to 0.10 m/s (approximately 20 m from the breakwater structure to the landward side area) and from 0.18 to 0.04 m/s (closest to the breakwater structure). The wave heights also decreased on the landward side of the breakwater from approximately 0.165 to 0.06 m. In addition, the current speeds slightly increased around the circulation gaps in the breakwater (CG1, CG2, CG3), above the stone (without L-blocks) and available gaps between the breakwater and earth dyke from 0.20 to 0.24 m/s due to the turbulent flows in these areas as the result of return flow occurrences, while the wave heights also increased slightly at the toe of the breakwater's main segment (S1, S2, S3) from 0.15 m to 0.18 m due to reflection incidences [41].

At the maximum tidal level during the spring tide, the water levels were higher than the breakwater's crest (the breakwater was submerged); consequently, the current and wave energies could pass through the study site via overtopping the structure. The overall current speed and wave heights on the landward side of the breakwater (mangrove degradation area) were reduced slightly from approximately 0.18 to 0.16 m/s and from 0.18 to 0.15 m, respectively. However, the current speeds on the landward side of the first main segment (S1) of the breakwater were found to be reduced by a greater amount, i.e., from 0.18 to 0.06 m/s. Additionally, current speeds and wave heights at the toe of the main body (direction the currents/waves come from) increased from 0.20 to 0.28 m/s and from 0.18 to 0.24 m, respectively. These increases might be due to refraction occurrences (due to the differences in water depths) combining with reflection incidences when the current and waves pass through the breakwater at an angle to underwater contours and through shallower depths [41].

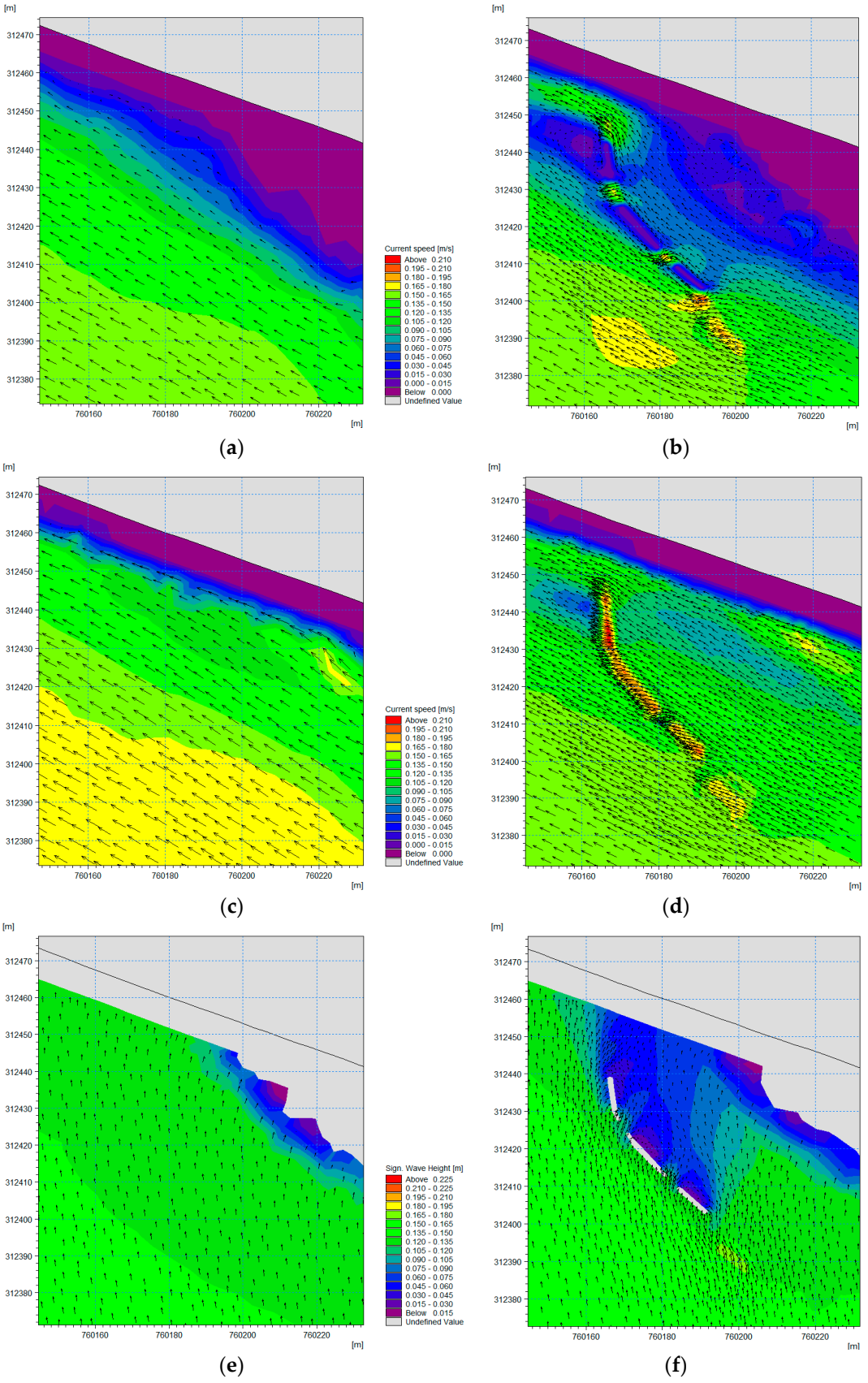

Figure 10. *Cont.*

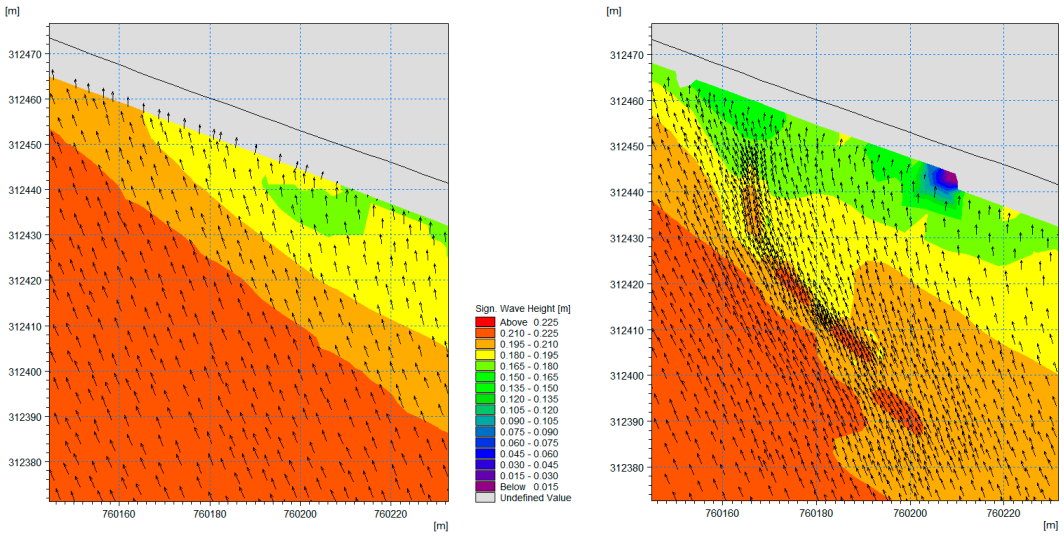

Figure 10. Simulated current and wave characteristics during the Southwest season: (**a**) CS during NT (WT); (**b**) CS during NT (W); (**c**) CS during ST (WT); (**d**) CS during ST (W); (**e**) SWH during NT (WT); (**f**) SWH during NT (W); (**g**) SWH during ST (WT); (**h**) SWH during ST (W). Notes: W = with breakwater, WT = without breakwater, CS = current speed, SWH = significant wave height, NT = neap tide, ST = spring tide.

(b) Changes in Current and Wave Characteristics during the Southwest Season (SW)

The simulation results shown in Figure 10 illustrate that without the coastal defence structure at the site, the currents flow to the degraded mangrove area from a Southeast direction approximately 120°–150° (magnetic) towards the Northwest direction with speeds between 0.09 and 0.18 m/s, while waves force the degraded mangrove area from the south between approximately 170° and 185° (magnetic) with significant heights of waves between 0.1 and 0.225 m during the Southwest season.

After construction of the breakwater in the intertidal area of Carey Island, the currents which flow from Southeast directions reach the degraded mangrove areas first, and then they flow seaward by overtopping the circulation gaps' of the breakwater (CG1, CG2, CG3) and through the available gaps between the breakwater and earth dyke or between the breakwater and stone (without L-blocks) during the neap tide. In this case, currents were reduced on the landward side of the breakwater structure from approximately 0.13 to 0.06 m/s, and they increased above the circulation gaps' structures and around the gaps between the breakwater and the stone (without L-blocks)/earth dyke from approximately 0.13 to 0.18 m/s. During the spring tide, the current speeds in the degraded mangrove area were reduced from 0.17 to 0.09 m/s, while the current speeds slowed quite significantly on the seaward side of the first main segment of the breakwater (S1), i.e., by up to approximately 0.04 m/s. In addition, the current speeds increased at the toe of the breakwater (direction the current comes from) from approximately 0.18 to 0.21 m/s.

In terms of the wave characteristics, the wave heights in the degraded mangrove area were reduced and concentrated on the landward side of the breakwater structure (from the middle structure to the earth dyke). Also, wave heights increased from 0.2 to 0.24 m at the toe of the breakwater and stones (without L-blocks). Such an increase in wave heights was due to refraction and reflection incidences as indicated by mechanics of wave motion in shore protection manual [41].

4.3. Suspended Sediment Transport in the Breakwater's Surroundings

Figure 11 presents the simulations of suspended sediment concentration during the NE season for the maximum tidal level of the neap tide and spring tide conditions in the vicinity of the breakwater. In addition, Figure 12 presents the simulations of suspended sediment concentration during the

SW season for the maximum tidal level of the neap tide and spring tide conditions around the breakwater structure.

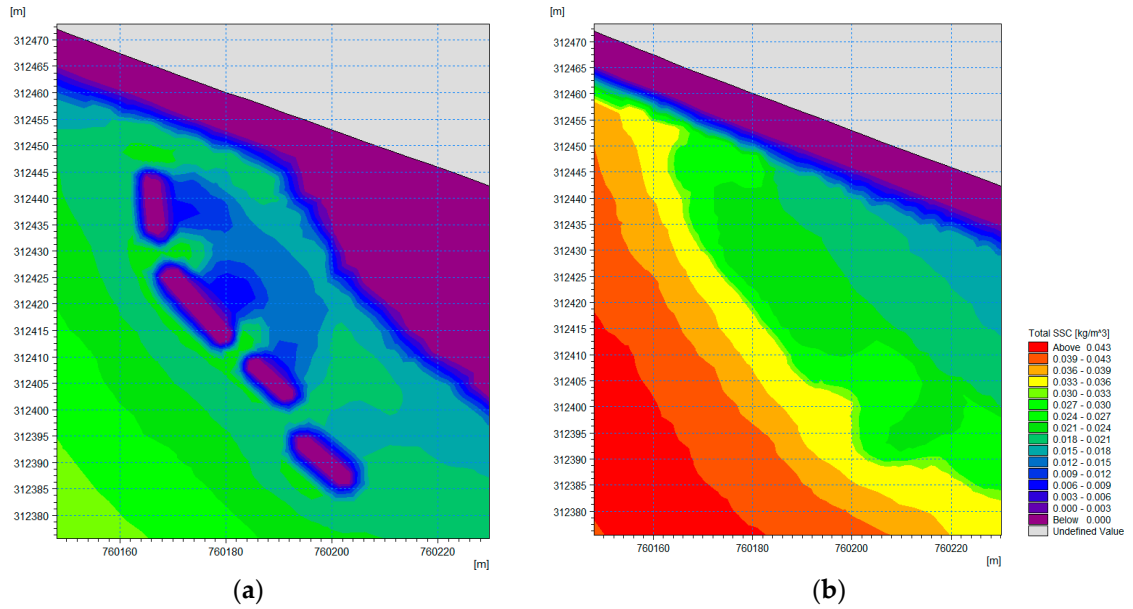

(**a**) (**b**)

Figure 11. Simulation of suspended sediment concentration during the Northeast season: (**a**) neap tide; (**b**) spring tide.

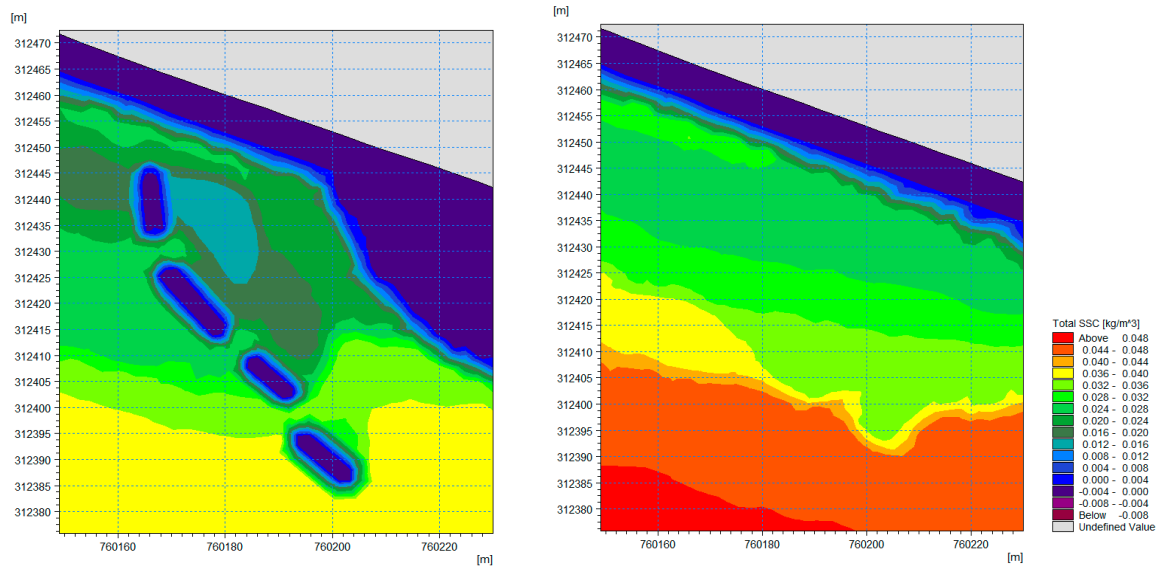

(**a**) (**b**)

Figure 12. Simulation of suspended sediment concentration during the Southwest season: (**a**) neap tide; (**b**) spring tide.

The average concentration of suspended sediment brought and transported by current and wave actions from the seaward side of the breakwater to the mangrove degradation area was approximately 0.048 kg/m^3, during the NE season (Figure 11) and 0.052 kg/m^3, during the SW season (Figure 12). Hence, there is a possibility that individual particles of the suspended sediments in water column become attached to each other and form flocks in the areas where the hydrodynamics conditions were calm enough. Based on the simulation results, the concentrations of suspended sediments brought from the seaward are slightly reducing in line with the mean wave direction towards the landward area. This result may have been obtained because some suspended sediment settles down on the sea-bed

due to the reduction of wave and current energies triggered by the high bottom friction coefficients of the cohesive sediments [30,31].

The simulation results of mud transport module (Figures 11 and 12) show that there are reductions in the SSC of the water column at the study site after the construction of the breakwater, especially in the landward area of the breakwater during the NE and SW seasons. In addition, reductions in the SSC are higher around the first main segment of the breakwater (S1) (seaward and landward areas) during the SW season.

4.4. Variation of Sea-Bed Levels and Erosion-Deposition Pattern in the Locality of the Low-Crested Breakwater

Figure 13 presents the variation of sea-bed levels and the pattern of erosion-deposition in the locality of the breakwater in the degraded environment, i.e., the cohesive intertidal area of Carey Island, measured every two months from December 2014 to October 2015.

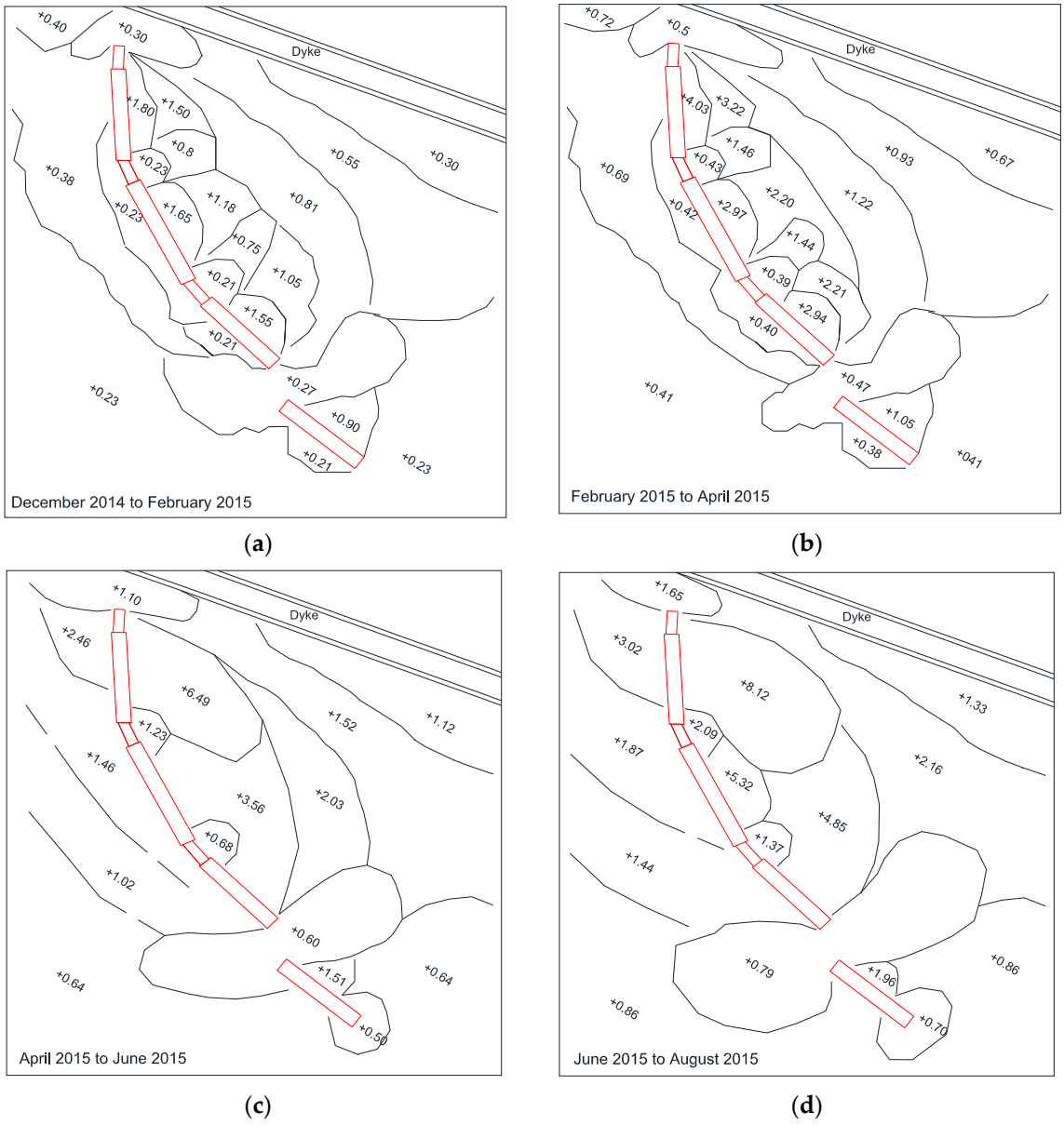

Figure 13. *Cont.*

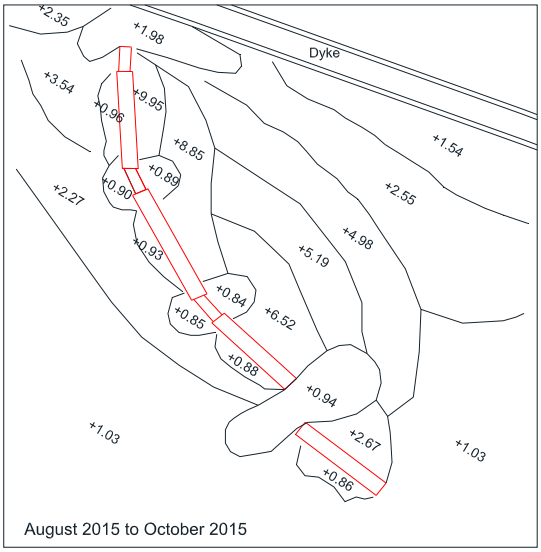

(**e**)

Figure 13. Variation of the sea-bed levels and erosion-deposition pattern in the locality of the breakwater structure over two-month periods from December 2014 to October 2015. Notes: + represents the deposition in cm, (**a**,**b**) NE season, (**c**,**d**,**e**) SW season.

The erosion-deposition patterns for the cohesive sediment in the intertidal area of Carey Island caused by the construction of the 85-m long, low-crested breakwater are evident. Unlike sand coasts, deposition patterns on cohesive coasts are more dynamic. Depositions are found to be higher at lower sea-bed elevations in protected areas with calm hydrodynamic conditions. Based on Figure 13, it is evident that there is an increment of sea-bed elevations in the degraded mangrove area after construction of the structure. During the NE season, the sediment accumulation rates were higher on the landward side of main segments of the breakwater (S1, S2, S3), while they were lower on the landward side of the circulation gaps' in the breakwater (CG1, CG2, CG3). During the SW season, the sediment accumulations are much higher surrounding the first main segment of the breakwater (S1), while lower amounts accumulate around the circulation gaps' in the breakwater and the gap between the breakwater and the stone (without L-blocks).

Overall, the sea-bed elevations in the degraded environment in the intertidal area of Carey Island increased by approximately 8 cm near to the first main segment of the breakwater (S1), while other areas on the landward side of the breakwater increased approximately 4 cm, on average, from December 2014 to October 2015.

4.5. Discussion

The hydrodynamic characteristics, cohesive behaviour of the sediments, concentration of suspended sediment and existence of a low-crest detached breakwater at the study site have resulted in specific patterns of sediment transport and erosion-deposition in the cohesive intertidal zone of Carey Island during both the SW and NE seasons.

4.5.1. Sediment Transport and Erosion-Deposition Pattern during the Northeast Season

Water flows from the nearshore area bring suspended sediments to the study site. Figures 9, 11 and 13 show the flow patterns, sediment transport and erosion-deposition in the locality of the detached breakwater during NE season. During the neap tide, the detached breakwater obstructs the transportation of some suspended sediments from the seaward side to the mangrove degradation area. It was found that the concentrations of suspended sediments are higher on the seaward side than the landward side of the breakwater. Some suspended sediments can enter the degraded mangrove

area through the gap between the breakwater and earth dyke or stone (without L-blocks) and also, by overtopping the circulation gaps' structure. The concentrations of suspended sediments in the water column were reduced further on the landward side of the breakwater because the sediment settles in this area due to the calm hydrodynamic conditions created by the breakwater and sediments are trapped [8,9].

During the spring tide, the suspended sediments from the seaward direction entered the degraded mangrove area via overtopping the breakwater structure. Some suspended sediments in the water column formed flocks and settle down in regions with lower hydrodynamic energies within the degraded mangrove area, while others were transported back seawards, all depending on turbulent properties resultant of the wave breaking and wave-current interactions. Suspended sediments containing flocks have higher settling velocities compared to individual particles; hence, they can settle and be deposited faster in regions with lower turbulent energies. The observed results were in line with the findings of previous studies conducted by Pejrup and Zhu et al. [37,38]. As current speeds and wave heights were reduced, the amount of sediment deposited increases in the landward area behind the breakwater, thus, the sediment accumulations were also higher during the NE season. The results were found to be in line with the field measurement (Figure 13a,b) which indicated that sediment accumulations were concentrated in the landward area behind the breakwater.

4.5.2. Sediment Transport and Erosion-Deposition Pattern during the Southwest Season

During the neap tide and spring tide in the SW season, the detached breakwater trapped suspended sediments before they flowed seaward from the degraded mangrove area. The suspended sediments settled in areas with lower hydrodynamic conditions, especially in the vicinity of the first main segment of the breakwater (S1). According to Figure 12, a lower amount of suspended sediment concentrations appeared around the first main segment of the breakwater (S1) due to the calmer hydrodynamic conditions (with current speeds of less than 0.07 m/s) and higher settling rate. The field measurement confirmed that sediment accumulations were concentrated around the first main segment of the breakwater structure and in the landward area behind the breakwater (Figure 13c–e).

Sediment accumulations were found to be slightly higher during the SW season compared to the NE season. This higher amount could be attributed to the calmer hydrodynamic conditions during the SW season. In addition, a higher amount of the suspended sediments were transported from the seaward to the study site during SW season. Calm hydrodynamic conditions and high suspended sediment concentrations could have accelerated the sediment deposition rate [4].

Finally, minor sea-bed elevation changes, with an average increment of 4 cm, were recorded in the landward area behind the breakwater after a year, which could have been influenced by the consolidation of the deposited cohesive sediment as indicated by several researchers as Kirby, Edmonds, & Ranasinghe [27,36,55,56].

5. Conclusions

The numerical modelling study showed that without having the breakwater in the degraded environment of the intertidal area, waves and curernts directly reach to the bare area at the study site with higher turbulent energy which means that in absence of the breakwater more intense degredation will occur in the coastal mangrove reserve area.

The numerical model found that the pattern of suspended sediment around the breakwater during both seasons is strongly affected by the local hydrodynamic conditions. It was shown that less energetic wave-current conditions effectively reduced the amount of SSC in the water column, as the suspended sediments were deposited in the water column under calm hydrodynamic conditions. In addition, the patterns of erosion-deposition in the locality of a low-crested breakwater on a cohesive coast were more dynamically evolving compared to a sandy coasts. Also, it was found that the deposition rate and sea-bed elevations increased more prominent under calm nearshore hydrodynamics.

Both field measurements and numerical modelling indicated that sediment accumulation increased in the degraded environment of the intertidal area of Carey Island with the presence of the detached breakwater. Field study showed increase in the sea-bed elevations, particularly near the first segment of breakwater structure. A smaller increased in bed elevations occured in the landward area behind the breakwaters. The results showed that the presence of the low-crested detached breakwater lead into sediment accumulations in the degraded environment in the intertidal area of Carey Island and reduce the erosion problem at the site. Sediment deposition during the calm seasons could create a suitable tidal regime for mangrove survival. The overall results indicated that conduction of the breakwater structure is vital to reduce the erosion problems in cohesive coasts of Carey Island and play a key role in success of mangrove rehabilitation projects in the region.

Author Contributions: A.F. and R.H. conceived and designed the study; A.F. performed data analyses; A.F. and S.A. wrote the manuscript; all authors (A.F., S.A., K.M. and R.H.) revised the manuscript for publication.

Funding: This work was funded by the High Impact Research, University of Malaya [Grant Number UM.C/HIR/MOHE/ENG/47] and the Ministry of Higher Education, Malaysia for TRGS/1/2015/UKM/02/5/1 & TRGS/1/2015/UKM/02/5/3.

Acknowledgments: The authors would like to thank the Department of Survey and Mapping Malaysia (JUPEM), the Department of Meteorology, Malaysia and the National Hydrography Centre, Malaysia for sharing the important data that enabled us to undertake this study.

Conflicts of Interest: The authors declare no conflict of interest.

References

1. Hashim, R.; Kamali, B.; Tamin, N.M.; Zakaria, R. An integrated approach to coastal rehabilitation: Mangrove restoration in Sungai Haji Dorani, Malaysia. *Estuar. Coast. Shelf Sci.* **2010**, *86*, 118–124. [CrossRef]
2. Hashim, R.; Fitri, A.; Motamedi, S.; Hashim, A.M. Modeling of Coastal Hydrodynamic Associated with Coastal Structures: A Review. *Malays. J. Sci.* **2013**, *32*, 149–154.
3. Scheffer, F. Rubble Mound Breakwaters for the New Port of Ennore (India)-Evaluation of Construction. Master's Thesis, Delft University of Technology, Delft, The Netherlands, 1999.
4. Saied, U.; Tsanis, I.K. A Coastal Area Morphodynamics Model. *Environ. Model. Softw.* **2008**, *23*, 35–49. [CrossRef]
5. Fairley, I.; Davidson, M.; Kingston, K. The Morpho-Dynamics of a Beach Protected by Detached Breakwaters in a High Energy Tidal Environment. *J. Coast. Res.* **2009**, *56*, 598–607.
6. Nam, P.T.; Larson, M.; Hanson, H. A Numerical Model of Beach Morphological Evolution Due to Waves and Currents in the Vicinity of Coastal Structures. *Coast. Eng.* **2011**, *58*, 863–876. [CrossRef]
7. Nam, P.T.; Larson, M.; Hanson, H. Modeling Morphological Evolution in the Vicinity of Coastal Structures. *Coast. Eng. Proc.* **2011**, *1*, 68. [CrossRef]
8. Barbaro, G.; Foti, G. Shoreline behind a Breakwater: Comparison between Theoretical Models and Field Measurements for the Reggio Calabria Sea. *J. Coast. Res.* **2012**, *29*, 216–224. [CrossRef]
9. Abolfathi, S.; Yeganeh-Bakhtiary, A.; Hamze-Ziabari, S.M.; Borzooei, S. Wave Runup Prediction Using M5′ Model Tree Algorithm. *Ocean Eng.* **2016**, *112*, 76–81. [CrossRef]
10. Fan, D.; Guo, Y.; Wang, P.; Shi, J.Z. Cross-Shore Variations in Morphodynamic Processes of an Open-Coast Mudflat in the Changjiang Delta, China: With an Emphasis on Storm Impacts. *Cont. Shelf Res.* **2006**, *26*, 517–538. [CrossRef]
11. Kamali, B. Design, Construction and Testing of L-Blok Detached Breakwater for Coastal Rehabilitation. Ph.D. Thesis, University of Malaya, Kuala Lumpur, Malaysia, 2011.
12. Wang, H.; Wang, A.; Bi, N.; Zeng, X.; Xiao, H. Seasonal Distribution of Suspended Sediment in the Bohai Sea, China. *Cont. Shelf Res.* **2014**, *90*, 17–32. [CrossRef]
13. Fitri, A.; Hashim, R.; Song, K.I.; Motamedi, S. Evaluation of Morphodynamic Changes in the Vicinity of Low-Crested Breakwater on Cohesive Shore of Carey Island, Malaysia. *Coast. Eng. J.* **2015**, *57*, 1550023. [CrossRef]
14. Pang, C.; Li, K.; Hu, D. Net Accumulation of Suspended Sediment and Its Seasonal Variability Dominated by Shelf Circulation in the Yellow and East China Seas. *Mar. Geol.* **2016**, *371*, 33–43. [CrossRef]

15. Zhang, H. Transport of Microplastics in Coastal Seas. *Estuar. Coast. Shelf Sci.* **2017**, *199*, 74–86. [CrossRef]
16. Joshi, S.; Xu, Y.J. Bedload and Suspended Load Transport in the 140-km Reach Downstream of the Mississippi River Avulsion to the Atchafalaya River. *Water* **2017**, *9*, 716. [CrossRef]
17. Fernández-Montblanc, T.; Izquierdo, A.; Quinn, R.; Bethencourt, M. Waves and Wrecks: A Computational Fluid Dynamic Study in an Underwater Archaeological Site. *Ocean Eng.* **2018**, *163*, 232–250. [CrossRef]
18. Dong, S.; Salauddin, M.; Abolfathi, S.; Tan, Z.H.; Pearson, J.M. The Influence of Geometrical Shape Changes on Wave Overtopping: A Laboratory and SPH Numerical Study. *Coasts Mar. Struct. Break.* **2018**, 1217–1226. [CrossRef]
19. Abolfathi, S.; Shudi, D.; Borzooei, S.; Yeganeh-Bakhtiari, A.; Pearson, J. Application of smoothed particle hydrodynamics in evaluating the performance of coastal retrofit structures. *Coast Eng. Proc.* **2018**. [CrossRef]
20. Dean, R.G.; Chen, R.J.; Browder, A.E. Full scale monitoring study of a submerged breakwater, Palm Beach, Florida, USA. *Coast. Eng.* **1997**, *29*, 291–315. [CrossRef]
21. Van Rijn, L.C. Coastal erosion and control. *Ocean Coast. Manag.* **2011**, *54*, 867–887. [CrossRef]
22. Sravanthi, N.; Ramakrishnan, R.; Rajawat, A.S.; Narayana, A.C. Application of Numerical Model in Suspended Sediment Transport Studies along the Central Kerala, West-Coast of India. *Aquat. Procedia* **2015**, *4*, 109–116. [CrossRef]
23. Archetti, R.; Zanuttigh, B. Integrated Monitoring of the Hydro-Morphodynamics of a Beach Protected by Low Crested Detached Breakwaters. *Coast. Eng.* **2010**, *57*, 879–891. [CrossRef]
24. Lamberti, A.; Zanuttigh, B. An Integrated Approach to Beach Management in Lido Di Dante, Italy. *Estuar. Coast. Shelf Sci.* **2005**, *62*, 441–451. [CrossRef]
25. Martinelli, L.; Zanuttigh, B.; Lamberti, A. Hydrodynamic and Morphodynamic Response of Isolated and Multiple Low Crested Structures: Experiments and Simulations. *Coast. Eng.* **2006**, *53*, 363–379. [CrossRef]
26. Zanuttigh, B. Numerical Modelling of the Morphological Response Induced by Low-Crested Structures in Lido Di Dante, Italy. *Coast. Eng.* **2007**, *54*, 31–47. [CrossRef]
27. Kirby, R. Chapter Four Distinguishing Accretion from Erosion-Dominated Muddy Coasts. In *Muddy Coasts of the World*; Healy, T., Wang, Y., Healy, J.A., Eds.; Elsevier: Amsterdam, The Netherlands, 2002; Volume 4, pp. 61–81.
28. Baas, J.H.; Davies, A.G.; Malarkey, J. Bedform Development in Mixed Sand–mud: The Contrasting Role of Cohesive Forces in Flow and Bed. *Geomorphology* **2013**, *182*, 19–32. [CrossRef]
29. Shi, Z.; Chen, J.Y. Morphodynamics and Sediment Dynamics on Intertidal Mudflats in China (1961–1994). *Cont. Shelf Res.* **1996**, *16*, 1909–1926. [CrossRef]
30. Birben, A.R.; Ozolcer, I.H.; Karasu, S.; Komurcu, M.I. Investigation of the effects of offshore breakwater parameters on sediment accumulation. *Ocean Eng.* **2007**, *34*, 284–302. [CrossRef]
31. United States Army, Corps of Engineers Coastal Engineering Research Center (U.S.). *Shore Protection Manual: Mechanics of Wave Motion: Volume 1, Chapter 2*; Department of the Army, Waterways Experiment Station: Washington, DC, USA, 1984.
32. Nikmanesh, M.R.; Talebbeydokhti, N. Numerical Simulation for Predicting Concentration Profiles of Cohesive Sediments in Surf Zone. *Sci. Iran.* **2013**, *20*, 454–465. [CrossRef]
33. Chang, K.H.; Tsaur, D.H.; Huang, L.H. Accurate Solution to Diffraction around a Modified V-Shaped Breakwater. *Coast. Eng.* **2012**, *68*, 56–66. [CrossRef]
34. De Jong, R.J. Wave Transmission at Low Crested Structures. Master's Thesis, Delf University of Technology, Delf, The Netherlands, 1996.
35. Young, D.M. A Laboratory Study on the Effects of Submerged Vertical and Semicircular Breakwaters on Near-Field Hydrodynamics and Morphodynamics. Master's Thesis, Clemson University, Clemson, SC, USA, 2008.
36. Edmonds, D.A.; Slingerland, R.L. Significant effect of sediment cohesion on delta morphology. *Nat. Geosci.* **2010**, *3*, 105. [CrossRef]
37. Pejrup, M.; Mikkelsen, O.A. Factors controlling the field settling velocity of cohesive sediment in estuaries. *Estuar. Coast. Shelf Sci.* **2010**, *87*, 177–185. [CrossRef]
38. Zhu, Z.; Yu, J.; Wang, H.; Dou, J.; Wang, C. Fractal dimension of cohesive sediment flocs at steady state under seven shear flow conditions. *Water* **2015**, *7*, 4385–4408. [CrossRef]
39. DHI. *MIKE 21 Mud Transport Scientific Documentation*; DHI Water and Environment: Hesholm, Denmark, 2014.

40. Jain, M. Wave Attenuation and Mud Entrainment in Shallow Waters. Ph.D. Thesis, University of Florida, Gainesville, FL, USA, 2007.
41. Yeganeh-Bakhtiary, A.; Houshangi, H.; Hajivalie, F.; Abolfathi, S. A Numerical Study on Hydrodynamics of Standing Waves in Front of Caisson Breakwaters with WCSPH Model. *Coast. Eng. J.* **2017**, *59*, 1750005-1–1750005-31. [CrossRef]
42. Abolfathi, S.; Pearson, J.M. Application of smoothed particle hydrodynamics (SPH) in nearshore mixing: A comparison to laboratory data. *Coast. Eng. Proc.* **2017**, *1*, 16. [CrossRef]
43. Eissa, S.S.; Lebleb, A.A. Numerical Modeling of Nearshore Wave Conditions at Al Huwaisat Island, KSA. *Aquat. Procedia* **2015**, *4*, 79–86. [CrossRef]
44. Patra, S.K.; Mohanty, P.K.; Mishra, P.; Pradhan, U.K. Estimation and Validation of Offshore Wave Characteristics of Bay of Bengal Cyclones (2008–2009). *Aquat. Procedia* **2015**, *4*, 1522–1528. [CrossRef]
45. Komen, G.J.; Cavaleri, L.; Donelan, M.; Hasselmann, K.; Hasselmann, S.; Janssen, P. *Dynamics and Modelling of Ocean Waves*; Cambridge University Press: Cambridge, UK, 1994.
46. Young, I. *Wind Generated Ocean Waves*; Elsevier: Amsterdam, The Netherlands, 1999; Volume 2.
47. Mehta, A.J.; Hayter, E.J.; Parker, W.R.; Krone, R.B.; Teeter, A.M. Cohesive sediment transport. I: Process description. *J. Hydraul. Eng.* **1989**, *115*, 1076–1093. [CrossRef]
48. Jose, F.; Stone, G.W. *Forecast of Nearshore Wave Parameters Using MIKE-21 Spectral Wave Model*; Gulf Coast Association of Geological Societies Transactions: Tulsa, OK, USA, 2006; Volume 56, pp. 323–327.
49. Jose, F.; Kobashi, D.; Stone, G.W. Spectral Wave Transformation over an Elongated Sand Shoal off South Central Louisiana, USA. *J. Coast. Res.* **2007**, *50*, 757–761.
50. Sørensen, O.R.; Kofoed-Hansen, H.; Rugbjerg, M.; Sørensen, L.S. A third-generation spectral wave model using an unstructured finite volume technique. *Coast. Eng.* **2004**, *4*, 894–906.
51. Department of Irrigation and Drainage. *Guideline for Hydrodynamic Modelling*; Department of Irrigation and Drainage: Kuala Lumpur, Malayisa, 2013.
52. DHI. *MIKE 21 Hydrodynamic Scientific Documentation*; DHI Water and Environment: Hesholm, Denmark, 2014.
53. DHI. *MIKE 21 Spectra Wave Scientific Documentation*; DHI Water and Environment: Hesholm, Denmark, 2014.
54. Song, J.; Wei, L.; Ming, Y. A method for simulation model validation based on Theil's inequality coefficient and principal component analysis. In Proceedings of the Asian Simulation Conference, Singapore, 6–8 November 2013; Springer: Berlin/Heidelberg, Germany, 2013; pp. 126–135.
55. Ranasinghe, R.; Turner, I.L. Shoreline response to submerged structures: A review. *Coast. Eng.* **2006**, *53*, 65–79. [CrossRef]
56. Ranasingle, R.; Larson, M.; Savioli, J. Shoreline response to a single shore-parallel submerged breakwater. *Coast. Eng.* **2010**, *57*, 1006–1017. [CrossRef]